



Effect of gauge-field interaction on fermion transport in two dimensions: Hartree conductivity correction and dephasing

T. Ludwig,¹ I. V. Gornyi,^{2,3,*} A. D. Mirlin,^{2,3,4,†} and P. Wölfle^{2,3,4}

¹*Instituut-Lorentz, Universiteit Leiden, P.O. Box 9506, 2300 RA Leiden, The Netherlands*

²*Institut für Nanotechnologie, Forschungszentrum Karlsruhe, 76021 Karlsruhe, Germany*

³*Center for Functional Nanostructures, Universität Karlsruhe, 76128 Karlsruhe, Germany*

⁴*Institut für Theorie der kondensierten Materie, Universität Karlsruhe, 76128 Karlsruhe, Germany*

(Received 14 April 2008; published 11 June 2008)

We consider the quantum corrections to the conductivity of fermions interacting via a Chern–Simons gauge field and concentrate on the Hartree-type contributions. The first-order Hartree approximation is only valid in the limit of weak coupling $\lambda \ll g^{-1/2}$ to the gauge field ($g \gg 1$ is the dimensionless conductance) and results in an antilocalizing conductivity correction $\sim \lambda^2 g \ln^2 T$. In the case of strong coupling, an infinite summation of higher-order terms is necessary, which includes both the virtual (renormalization of the frequency) and real (dephasing) processes. At intermediate temperatures, $T_0 \ll T \ll gT_0$, where $T_0 \sim 1/g^2\tau$ and τ is the elastic scattering time, the T dependence of the conductivity is determined by the Hartree correction, $\delta\sigma^H(T) - \delta\sigma^H(gT_0) \propto g^{1/2} - (T/T_0)^{1/2} [1 + \ln(gT_0/T)^{1/2}]$, so that $\sigma(T)$ increases with lowering T . At low temperatures, $T \ll T_0$, the temperature-dependent part of the Hartree correction assumes a logarithmic form with a coefficient of order unity, $\delta\sigma^H \propto \ln(1/T)$. As a result, the negative exchange contribution $\delta\sigma^{\text{ex}} \propto -\ln g \ln(1/T)$ becomes dominant, which yields localization in the limit of $T \rightarrow 0$. We further discuss dephasing at strong coupling and show that the dephasing rates are of the order of T , owing to the interplay of inelastic scattering and renormalization. On the other hand, the dephasing length is anomalously short, $L_\varphi \ll L_T$, where L_T is the thermal length. For the case of composite fermions with long-range Coulomb interaction, the gauge-field propagator is less singular. The resulting Hartree correction has the usual sign and temperature dependence, $\delta\sigma^H \propto \ln g \ln(1/T)$, and for realistic g is overcompensated by the negative exchange contribution due to the gauge-boson and scalar parts of the interaction. In this case, the dephasing length L_φ is of the order of L_T for not too low temperatures and exceeds L_T for $T \approx gT_0$.

DOI: [10.1103/PhysRevB.77.235414](https://doi.org/10.1103/PhysRevB.77.235414)

PACS number(s): 73.23.-b, 72.10.-d, 73.43.-f, 71.27.+a

I. INTRODUCTION

The problem of particles interacting with a transverse gauge field was first considered¹ in the context of the magnetic interaction of electrons in metals. It was found that such interactions lead to singular contributions to observables, since they are not screened, in contrast to the conventional interaction via a scalar potential. However, for the case of magnetic interactions of the electrodynamic origin, these effects are weak, since they are of relativistic nature. More recently, a two-dimensional (2D) version of the problem has attracted considerable interest² in connection with effective theories of strongly correlated systems, where gauge-field interactions lead to very strong effects: the gauge theory of high- T_c superconductors³ and, most prominently, the Chern–Simons theory of the half-filled Landau level.

In a field-theoretical description⁴ of 2D electrons in a strong magnetic field at half-filling of the lowest Landau level, electrons undergo a statistical transformation which transforms them into the so-called composite fermions by effectively attaching two flux quanta to each electron.⁵ As a result, the composite fermions strongly interact with a (fictitious) Chern–Simons gauge field. Although this gauge field vanishes on average at half filling, the density fluctuations of the electrons induce fluctuations of the gauge field. A treatment of these fluctuations has been developed in Ref. 6 (for reviews see, e.g., Refs. 7 and 8).

Due to the strong coupling of the fermions to the gauge field and the singular properties of the gauge field, the inter-

action effects can be much stronger and more complex than for the Coulomb interaction. For previous work, in this context, the reader is referred to Refs. 2 and 9–20. In particular, Refs. 10, 11, 14, 16, 18, and 19 have addressed questions related to dephasing phenomena and found unusually high dephasing rates, while Refs. 17 and 20 have considered the conductivity correction due to exchange interaction for such systems and predicted a negative correction to the conductivity varying as $\ln T$ at low temperatures with a nonuniversal prefactor logarithmically dependent on the resistivity. The experimental observation of such a correction has been reported in Ref. 21.

A new boost to the research in this direction was given by a recent work (Ref. 22). It was found there that the *positive* Hartree contribution to the quantum corrections to the density of states and to the conductivity dominates over the exchange contribution, therefore letting the system remain metallic at low temperatures. Most surprisingly, the Hartree contribution in Ref. 22 diverges in the limit of large systems, $L \rightarrow \infty$. If true, this would imply that the conductivity of such a system (in the thermodynamic limit) is infinite for sufficiently low temperatures. The very interesting and partly puzzling findings of Ref. 22 have served as one of the motivations of this work.

This paper presents a systematic analysis of the Hartree correction to the conductivity of a disordered fermion-gauge-field system. We start with a calculation of the first-order Hartree correction to conductivity in Sec. II. In Sec. II A, we

derive an effective interaction, which helps us to bring the considered contribution into a form similar to the usual exchange correction. At variance with Ref. 22, we find a natural low-momentum cutoff set by the diffusive dynamics, which ensures that gauge invariance is obeyed. This leads to a result for the conductivity correction, which is finite in the thermodynamic limit and positive, varying as $\ln^2 T$ with temperature. In Sec. II B, we elucidate the physical meaning of the obtained contribution. We show that it is governed by scattering on static mesoscopic fluctuations of local currents. To demonstrate this, we rederive the gauge-field-induced correction to the conductivity by using an earlier result for the correlation function of local mesoscopic currents.²³

When the interaction coupling constant λ is not too small (as, e.g., in the composite-fermion problem, where $\lambda \sim 1$), it is necessary to include higher orders of the interaction. Since the gauge-field interaction leads not only to renormalization but also to anomalously strong dephasing effects and since renormalization and dephasing get mixed in higher orders, we first discuss dephasing of Cooperons and diffusons coupled to a fluctuating gauge field.

In Sec. III A, we discuss the effect of dephasing on weak localization and find very short dephasing lengths, confirming earlier work.^{10,11,16,18} The physics of this strong dephasing, which is dominated by quasistatic gauge-field configurations, is also discussed there. We show a deep relation between dephasing of weak localization and mesoscopic conductance fluctuations in Sec. III B.¹⁹ Based on these results, the dephasing of diffusons with finite-delay times (which arise as elements of diagrams for the interaction-induced conductivity correction) is inspected in Sec. III C. In Sec. III D, we discuss the “true” dephasing rate governed by inelastic processes (rather than by ensemble averaging), which shows up in the two-loop weak-localization correction.

Using the results for dephasing of diffusons, we then construct a scheme to treat interaction effects to all orders. This starts with the treatment of large self-energies $\Sigma^Z \sim g\omega$, which we present in Sec. IV B. At low temperatures, $T \ll T_0$ (where $T_0 \sim 1/g^2\tau$, g is the dimensionless conductance and τ is the elastic scattering time) dephasing is not important and the strong renormalization effects lead to a low-frequency Hartree correction that is logarithmic in temperature with a coefficient of order unity,

$$\delta\sigma^H(T) \propto \ln(1/T). \quad (1.1)$$

This is accompanied by a high-frequency contribution that saturates to a constant (and is smaller than the Drude conductivity). As a result, the system of disordered fermions that interact through the gauge fields, while showing metalliclike behavior at sufficiently high T , eventually gets localized in the limit of lowest temperatures due to the negative exchange contribution finally overcompensating the Hartree contribution.

At intermediate temperatures $T_0 \ll T \ll gT_0$ (for $\lambda \sim 1$, higher temperatures are outside the diffusive regime, since the dephasing length L_φ becomes shorter than the mean free path l), dephasing and renormalization effects are both

present, and special care is needed to evaluate the Hartree contribution. We develop a proper method in Sec. IV C. The Hartree correction assumes the form

$$\delta\sigma^H(T) - \delta\sigma^H(gT_0) \propto g^{1/2} - \frac{T^{1/2}}{T_0^{1/2}} \left[1 + \frac{1}{2} \ln \frac{gT_0}{T} \right], \quad (1.2)$$

with the temperature dependence resulting from strong dephasing removing the contribution of low frequencies.

Taking into account the influence of the renormalization processes upon dephasing at strong coupling, we show in Sec. IV D that for $\lambda=1$, the dephasing rates are of the order of T . The renormalization of the frequency by virtual processes (inducing a strong Z factor, $Z \sim g$) compensates the large factor of g in the dephasing part of the self-energy. On the other hand, the dephasing length is anomalously short compared to the thermal length, $L_\varphi \ll L_T$.

Finally, in Sec. V, we turn to the model of composite fermions with an unscreened long-range Coulomb interaction. This suppresses charge fluctuations and leads⁶ to a less singular propagator of the gauge-field (which is induced by the density fluctuations via the Chern–Simons transformation). In this situation, the effect of the gauge-field interaction is much less dramatic: the large parameter g does not appear in the perturbative expressions for the dephasing rate as well as the first-order Hartree correction. As a result, formalism beyond first order (the resummation of higher-order gauge-field interaction terms) is not needed for realistic experimental parameters. Specifically, in Sec. V A, we find at not too low temperatures that the dephasing rate is of the order of the temperature and $L_\varphi \sim L_T$, while at the lowest temperatures, $L_\varphi \gg L_T$. Likewise, in Sec. V B, we find that the Hartree correction is positive and has the usual T dependence,

$$\delta\sigma^H \propto \ln g \ln(1/T), \quad (1.3)$$

with a small numerical prefactor. For realistic g , the total interaction correction is dominated by the gauge-field exchange contribution¹⁷ at intermediate temperatures and by the scalar part of the interaction²⁴ at the lowest T .

Our results are summarized in Sec. VI. Technical details are relegated to Appendixes A and F. Throughout the paper, we set $\hbar=1$.

II. SMALL COUPLING: FIRST-ORDER HARTREE CORRECTION

A. First-order Hartree diagrams

We consider a diffusive system of fermions in two dimensions that interact with a gauge field described by the transverse propagator,

$$U_{\alpha\beta}(\mathbf{k}, \epsilon) = \frac{1}{\chi_0 k^2 - i\sigma(k)\epsilon} \left[\delta_{\alpha\beta} - \frac{k_\alpha k_\beta}{k^2} \right], \quad (2.1)$$

where $\sigma(k)$ is the electric conductivity at finite wave vector \mathbf{k} and χ_0 is the magnetic susceptibility of the electrons. At small “diffusive” momenta $k \ll 1/l$ (where l is the elastic mean free path), the propagator takes the form

$$U_{\alpha\beta}(\mathbf{k}, \epsilon) \simeq \frac{1}{\sigma_0 k^2 l^2 T_0 - i\epsilon} \delta_{\alpha\beta}^\perp, \quad kl \ll 1. \quad (2.2)$$

Here, $\sigma_0 = e^2 \nu D$ is the Drude conductivity, D is the diffusion constant, and $\nu = m/2\pi$ is the density of states per spin (we do not account for the spin degree of freedom as appropriate for the fully polarized lowest Landau level). We have introduced the short notation

$$\delta_{\alpha\beta}^\perp \equiv \delta_{\alpha\beta} - k_\alpha k_\beta / k^2$$

for the transverse projector. Equation (2.2) has been written to display the characteristic temperature scale

$$T_0 = \frac{1}{12g^2\tau}, \quad (2.3)$$

where we have used the free-fermion susceptibility $\chi_0 = e^2/12\pi m$ resulting in $e^2 D/\chi_0 = 12\pi g$, and $g = 2\pi\sigma_0/e^2 = E_F\tau = k_F l/2$ is the dimensionless conductance. For ease of notation, we also define

$$T_n \equiv g^n T_0. \quad (2.4)$$

Propagator (2.2) corresponds to a short-range interaction (Coulomb interaction screened by, say, an external gate) of the electrons before the transformation into composite fermions. At the end of the paper, in Sec. V, we will investigate the case of unscreened Coulomb interaction.

The vertices coupling the gauge field to the fermions carry factors $e^* \mathbf{v}$, where at first, we allow the coupling constant e^* to be different from the electron charge e . This allows us to construct a well-controlled perturbation theory with a small parameter $\lambda = e^*/e$, although the results are not small in the usual parameter $1/g$. We will set the parameter λ to unity in Secs. IV B and IV C.

We will concentrate on systems with broken time-reversal symmetry. This is, in particular, the case for the half-filled lowest Landau level, where the external magnetic field and random potential of impurities induce, after the Chern-Simons transformation, a random magnetic field (RMF) as the dominant disorder for composite fermions.

We are interested in the Hartree contribution to the conductivity correction, which to leading order in the fermion-gauge-field coupling is given by the diagrams shown in Fig. 1. We consider the diffusive regime $T\tau \ll 1$ and do not treat the details of the diffusive-ballistic crossover, which involve some extra diagrams.^{25,26}

Defining the effective interaction \tilde{U} , as shown in Fig. 2 (see Appendix A), the Hartree diagrams with respect to the bare interaction $U_{\alpha\beta}$ can be written as exchange diagrams²² with respect to \tilde{U} (see Figs. 1 and 3). The two diagrams of Fig. 2 with the diffuson crossing the interaction line cancel the bare box at $k \ll q$ and are negligible at $k \gg q$. They thus provide a natural lower cutoff for the gauge-field momenta k , which has been missed in Ref. 22. In Appendix B, we derive the diagrams for the Hartree conductivity correction using a generating functional and show that all relevant diagrams involve the effective interaction block \tilde{U} as given by Fig. 2. It is also shown there that to the leading order, the Hartree conductivity correction can be equivalently represented ei-

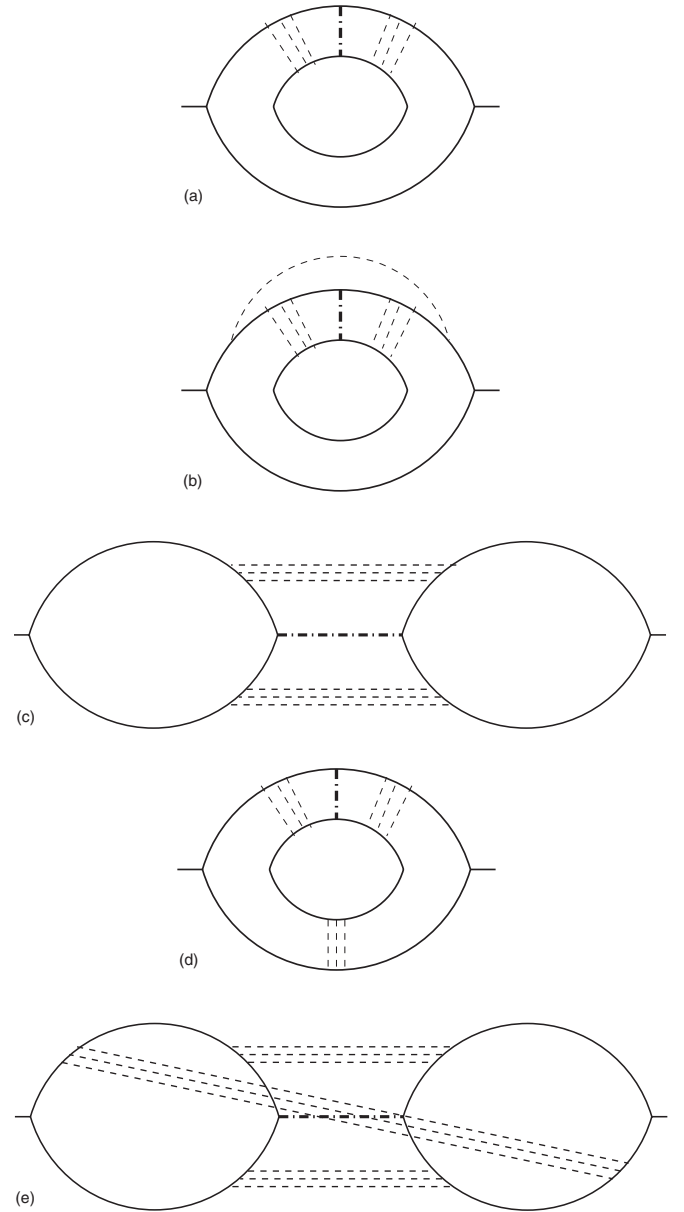


FIG. 1. Diagrams contributing to the Hartree part of the conductivity correction. The dashed lines represent impurities; the dotted-dashed line denotes the bare gauge-field propagator $U_{\alpha\beta}$ given by Eq. (2.1). Additionally, there is the possibility of diffusons crossing the gauge-field line, as shown in Fig. 2 and discussed in the text.

ther as a sum of diagrams (a) and (b) of Fig. 1 or a sum of diagrams (d) and (e) of Fig. 1, as in the case of conventional Coulomb interaction.²⁴

The effective interaction \tilde{U} is evaluated in Appendix A, with the result

$$\tilde{U}(q) \equiv \tilde{U}(q, \epsilon = 0) = \frac{3g\lambda^2}{\pi\nu} \ln \frac{1}{q^2 l^2}. \quad (2.5)$$

It is instructive to compare effective interaction block (2.5) with the dynamically screened Coulomb interaction $U_C(q, \omega)$ in the conventional interaction correction,²⁴

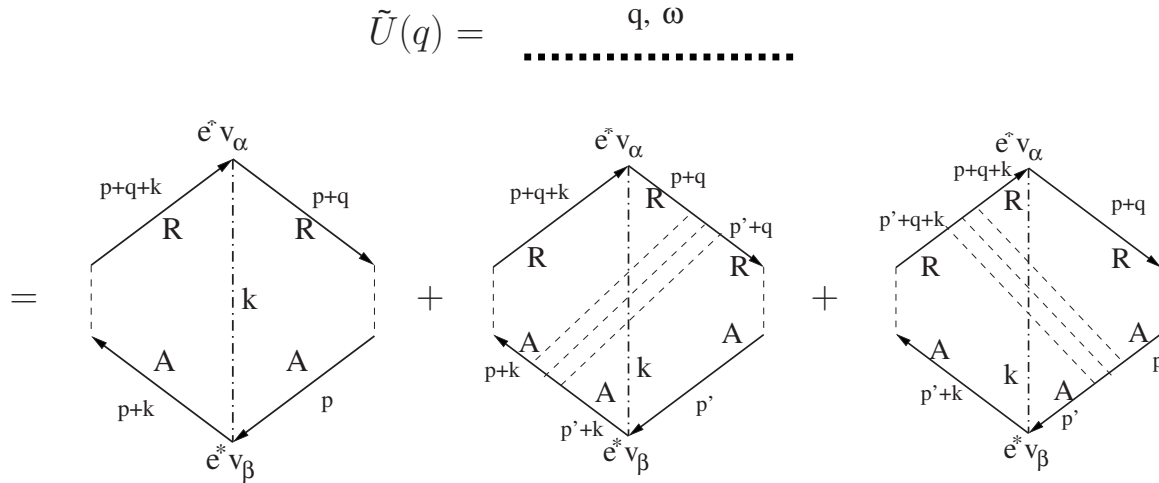


FIG. 2. Diagrams contributing to the effective interaction $\tilde{U}(q)$. The dotted-dashed line denotes the bare gauge-field propagator $U_{\alpha\beta}$. The two possibilities with the diffuson crossing the interaction line provide a natural low- k cutoff.

$$U_C(q, \omega) = \frac{1}{2\nu} \frac{Dq^2 - i\omega}{Dq^2}. \quad (2.6)$$

The main difference is the appearance of the parameter $g\lambda^2$ in the prefactor, which makes the effective gauge-field interaction block $\nu\tilde{U}(q) \sim g \gg 1$ very strong in the realistic case $\lambda=1$. Furthermore, for characteristic values of diffuson momenta and frequencies $Dq^2 \sim \omega$, the interaction $\tilde{U}(q)$ diverges logarithmically with decreasing q , while the screened Coulomb interaction can be replaced by a constant. Note that the gauge invariance ensures that the q^{-2} singularity of $U_C(q, \omega)$ at fixed ω does not lead to anomalies in the gauge-

invariant quantities such as the conductivity; see Refs. 25–29 for discussion.

Using the standard expression for the first-order exchange diagrams²⁴ (d) and (e) of Fig. 3,

$$\delta\sigma^H = 2\sigma_0 \int \frac{d\omega}{2\pi} \frac{\partial}{\partial\omega} \left[\omega \coth \frac{\omega}{2T} \right] \times \int (dq) \text{Im} \left\{ \tilde{U}(q) \frac{Dq^2}{(Dq^2 - i\omega)^3} \right\} \quad (2.7)$$

[we use the compact notation $\int (dq) \equiv \int d^2q / (2\pi)^2$] and the

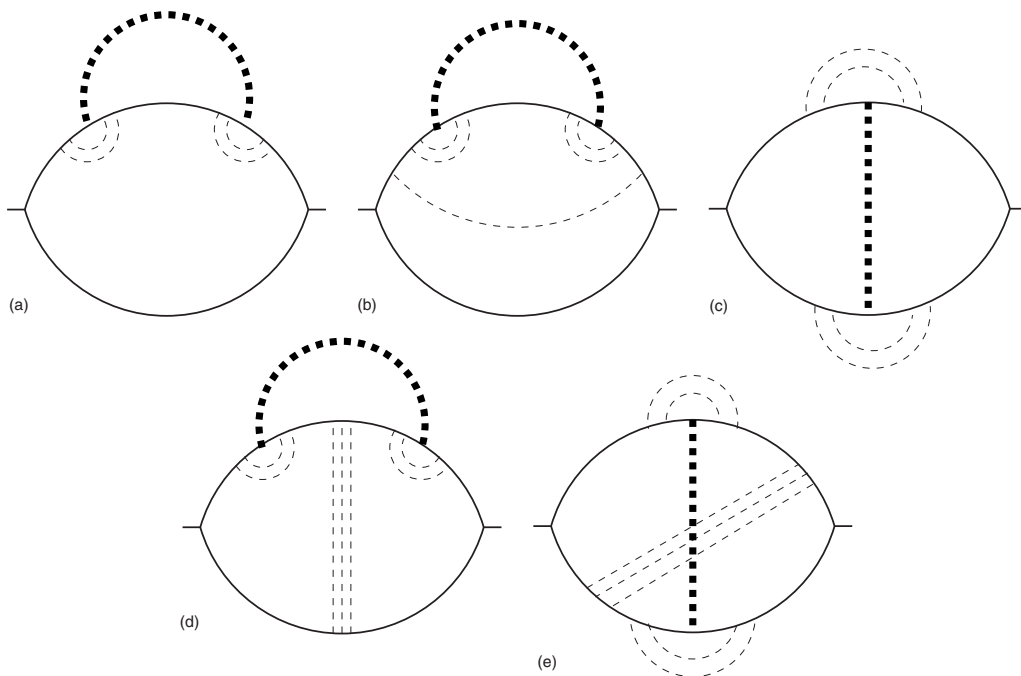


FIG. 3. Using the effective interaction \tilde{U} as defined in Fig. 2 (thick dotted line); the Hartree diagrams of Fig. 1 can be mapped onto the standard exchange diagrams of Ref. 24.

effective interaction $\tilde{U}(q)$ given by Eq. (2.5), we find the positive conductivity correction,

$$\begin{aligned} \delta\sigma^H &\approx \frac{3g(e^*)^2}{4\pi^3} \int_0^{1/\tau} \frac{d\omega}{\omega} \frac{\partial}{\partial\omega} \left[\omega \coth \frac{\omega}{2T} \right] \ln \frac{1}{\omega\tau} \\ &= \frac{3}{4\pi^2} \lambda^2 \sigma_0 \ln^2 \frac{1}{T\tau}. \end{aligned} \quad (2.8)$$

The correction is proportional to the parameter $\lambda^2 g$, as expected from the comparison of Eqs. (2.5) and (2.6). The stronger ($\ln^2 T$) temperature dependence as compared to the standard Altshuler–Aronov²⁴ interaction correction (which is proportional to $\ln T$) arises due to the logarithmic infrared singularity of effective interaction block (2.5). The overall sign is the result of including an additional minus sign relative to the standard formula for the exchange correction, due to the closed fermionic loop of the Hartree diagram. In Sec. II B, we will present another derivation reproducing Eq. (2.8).

The velocity factors at the interaction vertices introduce the factor g in effective interaction (2.5), which compensates the usual factor $1/g$, so that Eq. (2.8) is small compared to σ_0 only through the parameter λ . In the course of this paper, we will therefore develop more careful treatments beyond first order in the interaction in order to calculate the Hartree conductivity correction in the situation $\lambda=1$ relevant for the half-filled lowest Landau level.

Even though the relative Hartree conductivity correction $\delta\sigma^H/\sigma_0$ is not small in $1/g$, Eq. (2.8) does not diverge with the system size at variance with the results found in Ref. 22. This is because small gauge-field momenta $k \ll q$ are canceled (see Fig. 2 and Appendix A for details), so that a static uniform gauge field does not contribute to the correct effective interaction and gauge-invariance requirements^{9,12,13,23} are satisfied.

B. Alternative derivation of the Hartree correction from mesoscopic current fluctuations

In order to confirm Eq. (2.8) and shed more light on the underlying physics, we now provide an alternative derivation based on an existing result for the equilibrium current fluctuations in a disordered system without time-reversal symmetry. In Ref. 23, the following result for the correlation function of local mesoscopic currents has been derived for the relevant range $L_\omega^{-1} \ll k \ll l^{-1}$,

$$\langle j_\alpha(E+\omega) j_\beta(E) \rangle_k = \frac{e^2}{2\pi^3} \ln(kL_\omega) \delta_{\alpha\beta}^\perp, \quad (2.9)$$

with $L_\omega = (D/\omega)^{1/2}$. In the limit $k \rightarrow 0$, the current-current correlator vanishes as $(kL_\omega)^2$ (due to the gauge invariance), which is closely related to the infrared regularization of effective interaction (2.5). Equation (2.9) describes the upper part of Fig. 4 and similar diagrams. It can be identified as the Hartree correction to the tunneling density of states (TDoS) $\delta\nu^H$ (Fig. 5, which is generated by insertion of a scalar vertex into the lower part of Fig. 4 and similar diagrams with three diffusons), with the interaction line $U_{\alpha\beta}(k)$ removed.

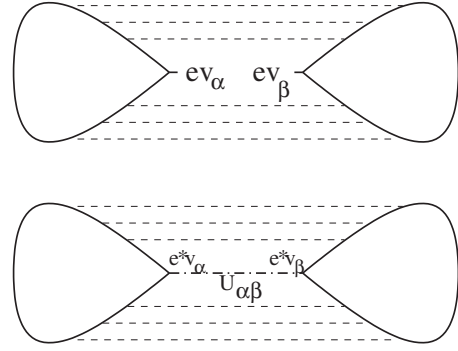


FIG. 4. Upper part: example of a contribution to the current correlator [Eq. (2.9)]. Lower part: the corresponding contribution to the current correlator can be obtained from the TDoS correction (Fig. 5, left) by removing the interaction line and the scalar vertex, while keeping the velocity vertices.

In analogy to Ref. 24, we consider the Hartree contribution to the energy shift of a state with unperturbed energy E_m above the Fermi sea (due to interactions with levels below the Fermi energy),

$$\begin{aligned} \Sigma_m^H &= \sum_{E_n < 0} \int d\mathbf{r} d\mathbf{r}' U_{\alpha\beta}(\mathbf{r} - \mathbf{r}') \\ &\quad \times \psi_m^*(\mathbf{r}) e^* \hat{v}_\alpha \psi_m(\mathbf{r}) \psi_n^*(\mathbf{r}') e^* \hat{v}_\beta \psi_n(\mathbf{r}'). \end{aligned} \quad (2.10)$$

Averaging over all states with this energy, the mean energy shift is

$$\begin{aligned} \Sigma_\epsilon^H &= \frac{(e^*)^2}{\nu V} \sum_m \langle \delta(\epsilon - E_m) \Sigma_m^H \rangle \\ &= \frac{(e^*)^2}{\nu V} \sum_m \langle \delta(\epsilon - E_m) \sum_{E_n < 0} \int d\mathbf{r} d\mathbf{r}' \\ &\quad \times U_{\alpha\beta}(\mathbf{r} - \mathbf{r}') \psi_m^*(\mathbf{r}) \hat{v}_\alpha \psi_m(\mathbf{r}) \psi_n^*(\mathbf{r}') \hat{v}_\beta \psi_n(\mathbf{r}') \rangle \\ &= \frac{(e^*)^2}{\nu V} \sum_m \int_\epsilon^\infty d\omega \langle \delta(\epsilon - E_m) \sum_{E_n < 0} \delta(\epsilon - \omega - E_n) \\ &\quad \times \int d\mathbf{r} d\mathbf{r}' U_{\alpha\beta}(\mathbf{r} - \mathbf{r}') \\ &\quad \times \psi_m^*(\mathbf{r}) \hat{v}_\alpha \psi_m(\mathbf{r}) \psi_n^*(\mathbf{r}') \hat{v}_\beta \psi_n(\mathbf{r}') \rangle \end{aligned}$$

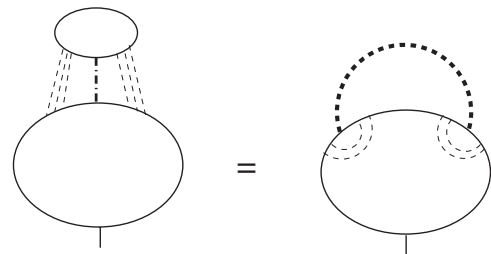


FIG. 5. The first-order correction to the TDoS [Eq. (2.16)].

$$= \frac{\lambda^2}{\nu} \int_{\epsilon}^{\infty} d\omega \int d(\mathbf{r} - \mathbf{r}') U_{\alpha\beta}(\mathbf{r} - \mathbf{r}') \langle j_{\alpha} j_{\beta} \rangle_{\mathbf{r}-\mathbf{r}', \omega}, \quad (2.11)$$

which after the Fourier transformation to momentum representation reads

$$\Sigma_{\epsilon}^H = \frac{\lambda^2}{\nu} \int_{\epsilon}^{\infty} d\omega \int (dk) U_{\alpha\beta}(\mathbf{k}) \langle j_{\alpha} j_{\beta} \rangle_{\mathbf{k}, \omega}, \quad (2.12)$$

with $U_{\alpha\beta}(\mathbf{k})$ given by Eq. (2.1). Using the formula

$$\frac{\delta \nu^H}{\nu} = - \frac{\partial \Sigma_{\epsilon}^H}{\partial \epsilon} \quad (2.13)$$

and the fact that

$$\frac{\delta \sigma^H}{\sigma_0} = \frac{\delta \nu^H(\epsilon \sim T)}{\nu} \quad (2.14)$$

(which can be directly shown by inserting velocity vertices into the diagrams for the TDoS correction), we find

$$\begin{aligned} \frac{\delta \sigma^H}{\sigma_0} &= \frac{\lambda^2}{\nu} \int (dk) U_{\alpha\beta}(\mathbf{k}) \langle j_{\alpha} j_{\beta} \rangle_{\mathbf{k}, T} \\ &= \frac{\lambda^2}{\nu} \int (dk) \frac{1}{\chi_0 k^2} \frac{e^2}{2\pi^3} \ln(kL_T) \\ &= \frac{\lambda^2 e^2}{4\pi^4 \nu \chi_0} \int_0^{\ln(L_T/l)} d \ln(kL_T) \ln(kL_T) \\ &= \frac{\lambda^2 e^2}{32\pi^4 \nu \chi_0} \ln^2 \frac{1}{T\tau}, \end{aligned} \quad (2.15)$$

which is identical to Eq. (2.8) since we have used the free-fermion relation $\nu \chi_0 = e^2 / 24\pi^2$.

The calculation in this section helps us to clarify the physical origin of the Hartree correction [Eqs. (2.8) and (2.15)]: this contribution to the conductivity is induced by scattering off static mesoscopic fluctuations of local currents, whose correlation function is given by Eq. (2.9). It is also instructive to explicitly calculate the first-order perturbative correction to TDoS (see Fig. 5),

$$\delta \nu^H(E) = - \frac{1}{\pi} \text{Im} \int (dp) \delta G^R(E, p). \quad (2.16)$$

Here, δG^R is the interaction-induced correction to the retarded Green's function of a fermion. For simplicity, we restrict ourselves to the zero- T case. Calculating the ‘‘exchange’’ correction using the effective interaction propagator \bar{U} given by Eq. (2.5), we need to include an additional minus sign due to the closed fermionic loop. After averaging over disorder, the first-order correction to the TDoS reads

$$\begin{aligned} \delta \nu^H(E) &\simeq \frac{1}{\pi} \frac{3\lambda^2 g}{\pi \nu} \text{Re} \int (dp) [G^R(E, p)]^2 G^A(E, p) \\ &\quad \times \int (dq) \int_E^{1/\tau} \frac{d\omega}{2\pi} \left[\frac{1}{\tau(Dq^2 - i\omega)} \right]^2 \ln \frac{1}{q^2 l^2} \\ &= \nu \lambda^2 \frac{3}{4\pi^2} \ln^2(E\tau). \end{aligned} \quad (2.17)$$

Thus, the Hartree correction to the conductivity and to the TDoS indeed has the same form [Eq. (2.14)] as expected.

Our aim now is to proceed on to the case where the coupling of the fermions to the gauge field (or, more precisely, the product $\lambda^2 g$) is not small, $\lambda^2 g \gg 1$, including the realistic case $\lambda = 1$. Since Eq. (2.15) is small only in the parameter λ^2 , it is necessary to take higher-order interaction effects into account. These involve dephasing (by real processes) and renormalization (by virtual processes). For a general review of these effects, we refer the reader to Refs. 30 and 31. Since dephasing effects in the present case^{10,11,16,18,19} are much stronger than in the standard situation^{30,32,33} even in the weak-coupling regime, we first study dephasing (at $\lambda^2 g \ll 1$) in detail in Sec. III. We return to the discussion of the Hartree correction to conductivity in Sec. IV B, where we will find that we may exclusively deal with renormalization effects at low temperatures. In Sec. IV C, we will then study the intermediate-temperature situation, where dephasing and renormalization compete. Finally, in Sec. IV D, we discuss the renormalization effects on the dephasing rate at strong coupling.

III. DEPHASING DUE TO WEAK GAUGE-FIELD FLUCTUATIONS

Even in a normal disordered metal, electrons are subject to transverse gauge-field fluctuations,^{24,32,34,35} however, the transverse part of the electromagnetic fluctuations is in that case small in v_F/c compared to the longitudinal one and may usually be neglected. In the composite-fermion model of the half-filled lowest Landau level,^{4,5} a situation occurs with a similar gauge-field propagator at the random-phase approximation (RPA) level,⁶ but a fermion-gauge-field coupling of order unity. Therefore, the effects of the gauge-field interaction may greatly exceed those of the Coulomb interaction.

The correlator of gauge-field fluctuations can be obtained according to the fluctuation-dissipation theorem from Eq. (2.1),

$$\langle a_{\alpha} a_{\beta} \rangle_{\mathbf{k}, \epsilon} = \coth \frac{\epsilon}{2T} \text{Im} U_{\alpha\beta}(\mathbf{k}, \epsilon). \quad (3.1)$$

In this section, we are interested in classical thermal fluctuations with $\epsilon \ll T$. The characteristic energy scale in Eq. (2.1) is $\epsilon \ll T_0$, while the corresponding transferred momenta \mathbf{k} fall into the diffusive range $k \ll 1/l$. This allows us to use Eq. (2.2) for $U_{\alpha\beta}(\mathbf{k}, \epsilon)$, yielding

$$\langle a_\alpha a_\beta \rangle_{\mathbf{k}, \epsilon} \approx \frac{2T}{\sigma_0} \frac{\delta_{\alpha\beta}^\perp}{(k^2 l^2 T_0)^2 + \epsilon^2}, \quad T \gg \epsilon. \quad (3.2)$$

Since the correlator is sharply peaked as a function of the transferred energy $\epsilon \lesssim T_0$, for many situations, the static approximation is appropriate, which collects all the weight in a δ function in energy space,

$$\langle a_\alpha a_\beta \rangle_{\mathbf{k}, \epsilon} = \frac{T}{\chi_0 k^2} \delta_{\alpha\beta}^\perp 2\pi \delta(\epsilon). \quad (3.3)$$

It is convenient to introduce the correlation function of the static vector potential,

$$\langle a_\alpha a_\beta \rangle_{\mathbf{k}} \equiv \frac{T}{\chi_0 k^2} \delta_{\alpha\beta}^\perp. \quad (3.4)$$

This corresponds to a static RMF with the correlator

$$\langle h(\mathbf{r})h(\mathbf{r}') \rangle = \frac{T}{\chi_0} \delta(\mathbf{r} - \mathbf{r}'). \quad (3.5)$$

Below, we use static approximation (3.3) whenever appropriate and return to the full dynamical form (3.2) if necessary [see discussion around Eqs. (3.25) and (3.32)]. It should be emphasized that the dephasing effects arising within the static approximation are purely geometric effects due to the phases associated with encircling magnetic flux and do not involve any energy transfer. The phase-space available for inelastic processes only appears through the magnitude of the correlation function of the RMF [Eq. (3.5)]. We will first discuss dephasing effects for Cooperons and conductance-fluctuation diffusons (which are the usual manifestations of the dephasing), and then refine the approach for a treatment of the (finite-delay time) diffusons appearing in the Hartree diagrams.

A. Cooperon dephasing

In this section, the Cooperon amplitude and the weak-localization correction are calculated for a system of fermions weakly coupled to a fluctuating gauge field ($\lambda^2 g \ll 1$). At variance with the rest of the paper where we concentrate on systems with broken time-reversal invariance (having composite fermions in mind as a particularly important example), here we consider the case of usual scalar-potential disorder that preserves the time-reversal symmetry. As discussed above, in the half-filled lowest Landau level, the time-reversal symmetry is broken by the static disorder acquiring a vector component via screening effects. Therefore, for the composite-fermion problem, the true Cooperon is completely suppressed by disorder-induced RMF. The analysis in this section should be then considered as an auxiliary calculation that helps to understand dephasing effects showing up in mesoscopic conductance fluctuations (Sec. III B).

The weak-localization correction to conductivity^{36–38} is given by

$$\delta\sigma_{\text{WL}} = -\frac{2e^2 D}{\pi} \int_{-\tau}^{\infty} dt \langle C^{t_0}(0,0;t,-t) \rangle, \quad (3.6)$$

where the Cooperon $C^{t_0}(\mathbf{r}, \mathbf{r}'; t, t')$ in the presence of a random gauge field satisfies

$$\begin{aligned} & \{ \partial_t + D[-i\nabla - \lambda e \mathbf{a}(\mathbf{r}, t_0 + t/2) \\ & \quad - \lambda e \mathbf{a}(\mathbf{r}, t_0 + t'/2)]^2 \} C^{t_0}(\mathbf{r}, \mathbf{r}'; t, t') \\ & = \delta(\mathbf{r} - \mathbf{r}') \delta(t - t'), \end{aligned} \quad (3.7)$$

and the average $\langle \dots \rangle$ is over the configurations of the random gauge field. The Cooperon $C^{t_0}(\mathbf{r}, \mathbf{r}'; t, -t)$ determining weak-localization correction (3.6) describes coherent propagation of a particle from \mathbf{r}' to \mathbf{r} and of a hole along the backward path from \mathbf{r} to \mathbf{r}' , with both processes starting at $t_0 - t/2$ and ending at $t_0 + t/2$. The averaged Cooperon does not depend on t_0 in view of translational invariance in time.

We write the Cooperon $C^{t_0}(0,0;t,-t)$ as a path integral,

$$C^{t_0}(0,0;t,-t) = \int_{\mathbf{r}(-t)=0}^{\mathbf{r}(t)=0} \mathcal{D}[\mathbf{r}(t')] \exp\{-S_0 + iS_1\}, \quad (3.8)$$

with the kinematic part of the action

$$S_0 = \int_{-t}^t dt' \frac{\dot{\mathbf{r}}^2(t')}{4D}, \quad (3.9)$$

which describes the diffusive dynamics, and

$$\begin{aligned} S_1 = & -\lambda e \int_{-t}^t dt' \dot{\mathbf{r}}(t') \cdot \mathbf{a}[\mathbf{r}(t_0 + t'/2)] \\ & - \lambda e \int_{-t}^t dt' \dot{\mathbf{r}}(t') \cdot \mathbf{a}[\mathbf{r}(t_0 - t'/2)]. \end{aligned} \quad (3.10)$$

Averaging over the gauge-field configurations with Gaussian weight, we have

$$\langle C^{t_0}(0,0;t,-t) \rangle = \int_{\mathbf{r}(-t)=0}^{\mathbf{r}(t)=0} \mathcal{D}[\mathbf{r}(t')] \exp\{-S_0 - \Delta S\}, \quad (3.11)$$

with [we now drop the “mute” variable t_0 and denote $C^{t_0}(0,0;t,-t) \equiv \mathcal{C}(t)$],

$$\begin{aligned} \Delta S(t) = & \frac{1}{2} \lambda^2 e^2 \int_{-t}^t dt_1 \int_{-t}^t dt_2 \dot{r}_\alpha(t_1) \dot{r}_\beta(t_2) \\ & \times \{ \langle a_\alpha[\mathbf{r}_1, t_1/2] a_\beta[\mathbf{r}_2, t_2/2] \rangle \\ & + \langle a_\alpha[\mathbf{r}_1, t_1/2] a_\beta[\mathbf{r}_2, -t_2/2] \rangle \\ & + \langle a_\alpha[\mathbf{r}_1, -t_1/2] a_\beta[\mathbf{r}_2, t_2/2] \rangle \\ & + \langle a_\alpha[\mathbf{r}_1, -t_1/2] a_\beta[\mathbf{r}_2, -t_2/2] \rangle \}, \end{aligned} \quad (3.12)$$

where $\mathbf{r}_i \equiv \mathbf{r}(t_i)$. Within the static gauge-field approximation as described by Eq. (3.3), Eq. (3.12) reduces to

$$\Delta S = 2\lambda^2 e^2 \int_{-t}^t dt_1 \int_{-t}^t dt_2 \dot{r}_\alpha(t_1) \langle a_\alpha[\mathbf{r}(t_1)] a_\beta[\mathbf{r}(t_2)] \rangle \dot{r}_\beta(t_2). \quad (3.13)$$

As discussed in the end of this section, the static approximation is sufficient for the present problem, except for very low temperatures, where some refinement will be needed. The time dependence of the gauge fields will, however, become crucial in Sec. III C where dephasing of “delayed diffusons” relevant to the Hartree correction will be analyzed.

It is convenient to define an effective action $\Delta S^{\text{eff}}(t)$ with the property¹⁸

$$\begin{aligned} \langle \mathcal{C}(t) \rangle &= \exp\{-\Delta S^{\text{eff}}(t)\} \int_{\mathbf{r}(-t)=0}^{\mathbf{r}(t)=0} \mathcal{D}[\mathbf{r}(t')] \exp\{-S_0\} \\ &= \exp\{-\Delta S^{\text{eff}}(t)\} \mathcal{C}^{(0)}(t), \end{aligned} \quad (3.14)$$

where $\mathcal{C}^{(0)}(t) \equiv (4\pi Dt)^{-1}$ is the unperturbed Cooperon in two dimensions. To second order in the coupling constant λe , $\Delta S^{\text{eff}}(t)$ can be evaluated as the average of ΔS weighted with the unperturbed Cooperon,

$$\Delta S^{\text{eff}}(t) \simeq \frac{1}{\mathcal{C}^{(0)}(t)} \int_{\mathbf{r}(-t)=0}^{\mathbf{r}(t)=0} \mathcal{D}[\mathbf{r}(t')] \exp\{-S_0\} \Delta S[\mathbf{r}(t'), t]. \quad (3.15)$$

The integral can be identified as the term of second order in λe of an expansion of the Cooperon $\mathcal{C} = (-D\nabla^2)^{-1} = (D\hat{\mathbf{q}}^2)^{-1}$

after coupling to the gauge field by the substitution $-i\nabla \rightarrow (-i\nabla - 2\lambda e\mathbf{a})$, $\hat{\mathbf{q}} \rightarrow (\hat{\mathbf{q}} - 2\lambda e\mathbf{a})$,

$$\begin{aligned} \mathcal{C} &= \mathcal{C}^{(0)} + 2\lambda e D \mathcal{C}^{(0)} \{a_\alpha, \hat{q}_\alpha\} \mathcal{C}^{(0)} - 4\lambda^2 e^2 D \mathcal{C}^{(0)} a_\alpha a_\alpha \mathcal{C}^{(0)} \\ &\quad + 4\lambda^2 e^2 D^2 \mathcal{C}^{(0)} \{a_\alpha, \hat{q}_\alpha\} \mathcal{C}^{(0)} \{a_\beta, \hat{q}_\beta\} \mathcal{C}^{(0)}, \end{aligned} \quad (3.16)$$

where $\{\cdot, \cdot\}$ is the anticommutator and summation over α and β is implied. In the static approximation, the two gauge-field terms in Eq. (3.7) simply add, so that the Cooperon couples with the charge $2\lambda e$ to the static gauge field.

Performing the average over the gauge-field fluctuations, we get

$$\begin{aligned} \langle \mathcal{C} \rangle &= \mathcal{C}^{(0)} - 4\lambda^2 e^2 D \mathcal{C}^{(0)} \langle a_\alpha a_\alpha \rangle \mathcal{C}^{(0)} \\ &\quad + 4\lambda^2 e^2 D^2 \mathcal{C}^{(0)} \langle \{a_\alpha, \hat{q}_\alpha\} \mathcal{C}^{(0)} \{a_\beta, \hat{q}_\beta\} \mathcal{C}^{(0)} \rangle. \end{aligned} \quad (3.17)$$

It is worth stressing that, within the approach based on Eq. (3.16), it is not necessary to distinguish to which fermionic line of the Cooperon the ends of the gauge-field line are connected. The reason is that within static approximation (3.3) for the gauge-field propagator, fermionic self-energy and vertex parts equally contribute, as can be seen from Eq. (3.7). This is at variance with the conventional case of scalar density-density interaction, where, both in Cooperon and diffuson, the fermionic self-energy and vertex interaction parts have opposite signs. In the present case of current-current interaction, the vertex interaction line in a Cooperon acquires an additional minus sign due to reversing the velocity in one of the fermionic lines constituting the Cooperon.

Employing static approximation (3.4), the averaged action $\langle \Delta S \rangle$ can thus be written as

$$\Delta S^{\text{eff}}(t) = \frac{1}{\mathcal{C}^{(0)}(t)} \int \frac{d\omega}{2\pi} \exp\{i\omega t\} \int (dq) \int (dk) \frac{1}{(D\mathbf{q}^2 - i\omega)^2} 4\lambda^2 e^2 D \left[-\langle a_\alpha a_\alpha \rangle_{\mathbf{k}} + \frac{4D}{D(\mathbf{q}-\mathbf{k})^2 - i\omega} \left(q - \frac{k}{2} \right)_\alpha \langle a_\alpha a_\beta \rangle_{\mathbf{k}} \left(q - \frac{k}{2} \right)_\beta \right]. \quad (3.18)$$

With gauge-field correlator (3.2), we find

$$\Delta S^{\text{eff}}(t) = 4\pi Dt \frac{4\lambda^2 e^2 DT}{\chi_0} \int \frac{d\omega}{2\pi} \exp\{i\omega t\} \int_0^{l^{-1}} \frac{qdq}{2\pi} \int_0^{l^{-1}} \frac{kdk}{2\pi} \int_0^{2\pi} \frac{d\phi}{2\pi} \frac{1}{(Dq^2 - i\omega)^2} \frac{1}{k^2} \left[-1 + \frac{4Dq^2 \sin^2 \phi}{Dq^2 - 2Dqk \cos \phi + Dk^2 - i\omega} \right], \quad (3.19)$$

where ϕ is the angle between the directions of the momenta \mathbf{q} and \mathbf{k} . An illustration of this equation is given in Fig. 6.

Equation (3.19) bears a close similarity to Eq. (21) of Ref. 18, which was derived in a different way (explicitly including ballistic propagation). Here, the first term (-1) in brackets takes the role of the ballistic term of Ref. 18. The cancellation of the two terms in brackets at $\omega=0$ and $k \rightarrow 0$ is a result of gauge invariance: A static uniform gauge field should not affect observables. This cancellation is the path-integral counterpart of the cancellation in the effective interaction box \tilde{U} (Fig. 2) in the Hartree correction (Sec. II).

Inspection of Eq. (3.19) shows that the k integral is logarithmic in the range $q < k < l^{-1}$, with the second term in the brackets providing the low- k cutoff at $k \sim q$. Evaluating then q integrals in Eq. (3.19), we find

$$\Delta S^{\text{eff}}(t) = \frac{24}{\pi} \lambda^2 g T t \int_0^\infty d\omega \frac{\sin \omega t}{\omega} \ln \frac{L\omega}{l}. \quad (3.20)$$

Setting $\omega \sim 1/t$ under the logarithm, we evaluate Eq. (3.20) with logarithmic accuracy, arriving at

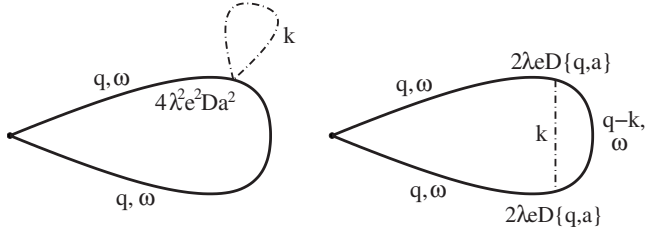


FIG. 6. Illustration of the processes contributing to Eqs. (3.18) and (3.19). The left and right diagrams give the first and second terms in brackets, respectively.

$$\Delta S^{\text{eff}}(t) = 6\lambda^2 g T t \ln \frac{t}{\tau}, \quad (3.21)$$

which is in agreement with Ref. 18. Let us note that in Ref. 18, this result was obtained by explicitly treating the ballistic dynamics in a particular model of isotropic scattering. On the other hand, we have derived Eq. (3.21) within a purely diffusive calculation without the need of taking details of ballistic propagation into account. This could be expected since the relevant physics happens on the large length scales of diffusive propagation and does not depend on the details of microscopic scattering processes.

The physical picture behind Eq. (3.21) is the following: For a typical closed diffusive path, the *geometrical* area covered by it will be proportional to its duration t , and so will be the average absolute value of the flux through this area, suggesting $\langle \Delta S \rangle(t) \propto t$. However, the path may encircle some areas more than once. Since the gauge-field configuration does not appreciably change during the time in between, the phases picked up from that area will coherently add up, so that the quantity relevant for dephasing is the *nonoriented* (Amperean) area enclosed, with the result^{10,11}

$$\Delta S = \frac{2\lambda^2 e^2 T}{\chi_0} \sum_i n_i^2 A_i, \quad (3.22)$$

where $n_i \in \mathbb{Z}$ is the number of times the area A_i is encircled. Reference 11 then proceeded by setting all $n_i = 1$, which approximates the nonoriented area $\sum_i n_i^2 A_i$ by the geometrical area $A = \sum_i A_i \sim Dt$ to obtain a linear-in- T dephasing rate, $1/\tau_\varphi \sim \lambda^2 g T$. The logarithmic correction in Eq. (3.21) is thus due to diffusive paths forming multiple loops.

The dephasing rate $1/\tau_\varphi$ and corresponding dephasing length $L_\varphi = (D\tau_\varphi)^{1/2}$ (note that this relation between τ_φ and L_φ only holds for weak coupling $\lambda^2 g \ll 1$; see Sec. IV D) can be defined using Eq. (3.21) and the condition $\Delta S^{\text{eff}}(t = \tau_\varphi) = 1$,

$$\frac{1}{\tau_\varphi} = 6\lambda^2 g T \ln \frac{T_1}{\lambda^2 T}, \quad T_0/\lambda^2 g \ll T \ll T_1/\lambda^2. \quad (3.23)$$

The weak-localization correction is now easily calculated,

$$\begin{aligned} \delta\sigma_{\text{WL}} &= -\frac{2e^2 D}{\pi} \int_\tau^\infty dt \langle C(t) \rangle \\ &= -\frac{2e^2 D}{\pi} \int_\tau^\infty dt C^{(0)}(t) \exp\{-\Delta S^{\text{eff}}(t)\} \\ &= -\frac{e^2}{2\pi^2} \ln \frac{\tau_\varphi(T)}{\tau}. \end{aligned} \quad (3.24)$$

At higher temperatures, $T \gtrsim T_1/\lambda^2$, the weak-localization amplitude is dominated by very short Cooperon paths of duration $t \lesssim \tau$, so that the present calculations for the diffusive regime do not apply. We do not attempt an analysis of the diffusive-ballistic crossover and of the ballistic regime in this paper.

At sufficiently low temperatures, $T \ll T_0/\lambda^2 g$, the fully static approximation is no longer valid, since the characteristic times $t \sim \tau_\varphi$ in the Cooperon propagator become longer than $1/T_0$ [see also the discussion below Eq. (3.37)]. At such long times, the correlations between the forward and backward interfering paths disappear due to the slow dynamics of the gauge fields: only two out of four terms in Eq. (3.12) survive, which are related to the correlations within the same (forward or backward) path. For those remaining correlations, the static approximation still applies, as long as $T > T_0$. As a result, at $T \ll T_0/\lambda^2 g$, the dephasing action becomes smaller than Eq. (3.21) by a factor of 2, yielding

$$\frac{1}{\tau_\varphi} = 3\lambda^2 g T \ln \frac{T_1}{\lambda^2 T}, \quad T_0 \ll T \ll T_0/\lambda^2 g. \quad (3.25)$$

Note that this intermediate regime disappears in the strong-coupling regime $\lambda^2 g \gg 1$.

At the lowest temperatures $T < T_0$, the result is further modified by the fact that the allowed phase space for the inelastic energy transfers, $|\epsilon| \lesssim T$, does not cover the whole peak of correlator (3.2). This results in the appearance of the ratio T/T_0 under the logarithm in the dephasing action,

$$\Delta S^{\text{eff}}(t) = 3\lambda^2 g T t \ln \frac{Tt}{T_0 \tau}, \quad T \ll T_0, \quad (3.26)$$

which, in turn, makes the logarithmic factor in the dephasing rate T independent,

$$\frac{1}{\tau_\varphi} = 3\lambda^2 g T \ln \frac{g}{\lambda^2}, \quad T \ll T_0. \quad (3.27)$$

The above results for the dephasing rate are only valid in the regime of weak coupling $\lambda^2 g \ll 1$. For stronger coupling, including the realistic case $\lambda = 1$, one should take into account the renormalization of the interfering paths by virtual processes, which are reflected in the strong interaction-induced Z factor in the Cooperon propagators. This situation is discussed in Sec. IV D below.

Since the logarithmic correction in Eq. (3.21) is the result of multiple return processes, it is instructive to make a short digression and to inspect ΔS^{eff} for a quasi-one-dimensional (quasi-1D) wire of width $w \gg l$. In that situation, the Cooperon dephasing rate is¹⁹

$$\frac{1}{\tau_\varphi} = 24\lambda^2 g_\square T \ln \frac{w}{l}, \quad T \ll T_1/\lambda^2 \quad (3.28)$$

(g_\square is the conductance per square), without any infrared anomalies. Equation (3.28) results from a linear-in- t behavior of ΔS^{eff} , which consists of a factor $t^{1/2}$ from the normalization of the unperturbed quasi-one-dimensional Cooperon and an *algebraic* correction factor $t^{1/2}$ due to the enhancement of the nonoriented area over the geometric one. In view of the absence of infrared divergences, the different behavior of dephasing rates associated with the Aharonov–Bohm oscillations in quasi-1D rings³⁹ and weak localization in quasi-1D wires, due to different low-momentum cutoff conditions, does not occur for the dephasing by gauge-field fluctuations.¹⁹

B. Diffuson dephasing: Mesoscopic conductance fluctuations

We now turn to the dephasing applicable to mesoscopic conductance fluctuations.^{40–45} Later on, we will relate it to the treatment of Cooperon dephasing within the context of weak localization (Sec. III A) and of the delayed-diffuson dephasing (Sec. III C) relevant for Hartree conductivity correction. The variance of the conductance can be written as

$$\begin{aligned} \langle \delta g^2 \rangle &= \frac{16\pi D^2}{3TL^4} \int d\mathbf{r}_1 d\mathbf{r}_2 \int dt dt' \tilde{\delta}(t-t') \\ &\times \langle \mathcal{D}^{12}(\mathbf{r}_1, \mathbf{r}_2, t) \mathcal{D}^{21}(\mathbf{r}_2, \mathbf{r}_1, t') \rangle, \end{aligned} \quad (3.29)$$

where L is the system size, the function $\tilde{\delta}(t-t')$ describes the thermal smearing of the two Fermi distribution functions,

$$\begin{aligned} \tilde{\delta}(t-t') &= 12\pi T \int \frac{d\epsilon_1 d\epsilon_2}{2\pi 2\pi} f'(\epsilon_1) f'(\epsilon_2) \exp\{i(\epsilon_1 - \epsilon_2)(t-t')\} \\ &= 3\pi T^3 (t-t')^2 \sinh^{-2}[\pi T(t-t')] \end{aligned} \quad (3.30)$$

[which for $T(t-t') \gg 1$ may be replaced by a true delta function] and \mathcal{D}^{12} is a diffuson satisfying

$$\begin{aligned} \{\partial_t + D[-i\nabla - \lambda \mathbf{e}_1(\mathbf{r}, t) + \lambda \mathbf{e}_2(\mathbf{r}, t)]^2\} \mathcal{D}^{12}(\mathbf{r}, \mathbf{r}', t) \\ = \delta(\mathbf{r} - \mathbf{r}') \delta(t). \end{aligned} \quad (3.31)$$

Here, the two measurements denoted by 1, 2; see uncorrelated gauge-field configurations. In the absence of interaction-induced dephasing [$\mathbf{a}_i(\mathbf{r}, t) = 0$], Eqs. (3.29)–(3.31) lead to the famous universal conductance fluctuations (UCFs), $\langle \delta g^2 \rangle \sim 1$, which are independent of the system size (only dependent on its dimensionality and shape). Dephasing manifests itself in a suppression of conductance fluctuations as compared to the fully coherent UCF regime.

Since the “UCF diffuson” \mathcal{D}^{12} involves two separate measurements, it is not subject to particle number conservation.³³ In other words, the cancellation between self-energy and vertex corrections known from the “true” diffuson does not occur since vertex corrections, with an interaction line connecting the fermionic lines, are absent: A truly static random magnetic field would indeed drop out of Eq. (3.31); however, a slowly varying random gauge field does not drop out when

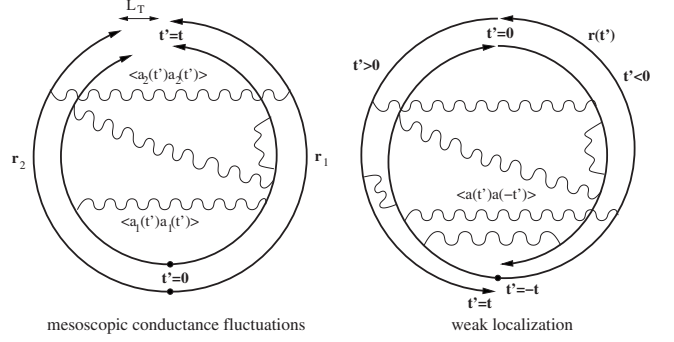


FIG. 7. Illustration of the path-integral transformation, which related weak localization to mesoscopic conductance fluctuations. The detailed presentation of the transformation can be found in Appendix C. As indicated in the left part of this figure, the two paths only need to end within one thermal length L_T of each other, changing the short-scale cutoff in Eq. (3.32) (see Ref. 33). For mesoscopic conductance fluctuations, vertex corrections (interaction lines connecting the two copies of the same path) are absent. For the Cooperon (right part of the figure), the vertex corrections are present and add to the self-energy terms.

the diffuson is formed by two Green’s functions related to two separate measurements.

The essential ingredient of the calculations is the following assumption about the time scales involved: Characteristic frequencies of the gauge-field fluctuations are much smaller than those of the electron diffusion, so that to a good approximation, a fermion experiences a static random gauge field while diffusing through the sample. The duration of a measurement, in turn, is assumed to be much longer than the time scale set by the gauge-field fluctuations, so that a measurement samples many electrons and performs a complete ensemble average over realizations of the random gauge field. Finally, different measurements will see no correlation between their respective gauge-field configurations. Technically, this means that static gauge-field correlator (3.3) is used for correlations experienced by any individual fermion, and correlators between separate measurements are completely dropped.

The aim of this section is to establish a formal relation between weak localization and mesoscopic conductance fluctuations when the dephasing is governed by a fluctuating gauge field. A relation of this kind has been demonstrated for the case of the usual screened Coulomb interaction by Aleiner and Blanter.³³ It has been formulated in a more general way in Ref. 39 (and more recently also been confirmed independently⁴⁶), where it has been shown that a manipulation of the path-integral expressions can transform these quantities one into another without actually evaluating the path integrals. When applied to a ring geometry, this general relation links h/e (mesoscopic) and $h/2e$ (weak-localization) Aharonov–Bohm oscillations.^{19,39}

We now present a similar calculation for the case of a fluctuating gauge field. This situation differs in the following points from the case of the screened Coulomb interaction: First, the characteristic time scales of the gauge field are much longer than the time scales of diffusion. This is important because, as will be discussed below, it results in an

ensemble-averaging effect that suppresses mesoscopic conductance fluctuations but not weak localization. On the other hand, weak localization is suppressed by the time-reversal symmetry breaking due to the fluctuating gauge field, while mesoscopic conductance fluctuations are insensitive to time-reversal breaking once it has resulted in the transition from the orthogonal to the unitary symmetry class.

The detailed path-integral transformation is performed in Appendix C and illustrated in Fig. 7. The results have slightly different forms depending on temperature ranges. For temperatures $T > T_0/\lambda^2 g$ (the range of validity of the static approximation for the Cooperon dephasing), the thermal prefactor can be written for $T \gg D/L^2$,

$$\langle \delta g^2 \rangle(T) = \frac{2\pi D}{3TL^2} |\delta g_{\text{WL}}|_{T \rightarrow T/2, l \rightarrow L_T} = \frac{2D}{3TL^2} \ln[T\tau_\varphi(T/2)], \quad (3.32)$$

where the dimensionless conductance correction $\delta g_{\text{WL}} = 2\pi\delta\sigma_{\text{WL}}/e^2$ is given by Eq. (3.24) and the dephasing rate $1/\tau_\varphi(T)$ is given by Eq. (3.23). Equation (3.32) is the equivalent of Eqs. (38) and (50) of Ref. 33 which were derived for the standard screened Coulomb interaction.

The essential feature of Eq. (3.32) is that the interaction via a static gauge field has given rise to a relative factor of 1/2 in the temperature argument of the dephasing time. The reason is that for the case of conductance fluctuations, half of the possible gauge-field correlators are between the two different measurements, so that only the other half of them remain. This issue does not appear in the standard situation because the correlator of the screened Coulomb interaction is not slow but local in time. At lower temperatures, $T < T_0/\lambda^2 g$ [when $\tau_\varphi(T) \gg 1/T_0$], the fully static approximation is no longer valid. The Cooperon dephasing rate [Eqs. (3.25) and (3.27)] becomes then twice smaller and the relative factor of 1/2 in Eq. (3.32) disappears.

The replacement $l \rightarrow L_T$ is due to the different short-scale cutoffs of the two quantities involved: Mesoscopic conductance fluctuations are given by pairs of paths which end within a distance of $L_T \equiv (D/T)^{1/2}$ of each other, while combining them to one closed loop, as needed for weak localization, requires them to end within one mean free path of each other. This modification has no effect in $d=1$ and only enters logarithmically in $d=2$. In Ref. 33, where the case of Coulomb interaction has been considered, this has been formulated using differences of the quantities on both sides, taken at different fields, so that the logarithmic cutoff drops out.

Equation (3.32) states that, also in the presence of a fluctuating gauge field, there is a deep relation between weak localization and mesoscopic conductance fluctuations, which is similar to the ones found in Refs. 19 and 33, and that these two quantities feature essentially the same dephasing rates. The time-reversal breaking effect of the gauge field on weak localization is mapped onto the ensemble-averaging effect of slowly varying gauge-field configurations on mesoscopic conductance fluctuations. For many conceptual purposes, it is therefore convenient to study whichever of these two quantities is more accessible.

A generalization of these formulas involving the correlation between conductances at two magnetic field values and diffuson and Cooperon contributions with the difference and the sum of the magnetic field arguments appearing is straightforward in analogy to Ref. 33. Since the connection between mesoscopic conductance fluctuations and weak localization has been made on the path-integral level, the corresponding generalizations to h/e and $h/2e$ Aharonov–Bohm oscillations are straightforward, as in the standard case.^{19,33,39}

C. Delayed-diffuson dephasing

While the Cooperon and the UCF diffuson are dephased by all gauge-field fluctuations, it is well known that a true diffuson is subject to particle number conservation. More precisely, while the total number of particles is conserved, the number of particles with given energy is not conserved if inelastic processes are taken into account. Then, the diffuson at fixed particle energy acquires a dephasing rate, which cuts off the infrared singularity. In position-time representation, the energy dependence of the diffuson transforms into a dependence on the delay time η between the particle and hole propagators. In the limit of $\eta \rightarrow 0$, corresponding to integration over all energies, the full diffusion pole is restored.

The diffusons in the Hartree interaction diagrams have this intermediate character: Since they connect two different fermionic bubbles, and the gauge field has much slower dynamics than the diffusion processes, these diffusons allow for a delay time between the fermionic lines. A related situation has been investigated in Ref. 47 in the context of the second-loop weak localization and its dephasing due to the Coulomb interaction.

In the presence of a fluctuating gauge field, the delayed diffuson satisfies the equation

$$\{\partial_t + D[-i\nabla - \lambda e\mathbf{a}(\mathbf{r}, t + \eta/2) + \lambda e\mathbf{a}(\mathbf{r}, t - \eta/2)]^2\} \mathcal{D}_\eta(\mathbf{r}, \mathbf{r}', t) = \delta(\mathbf{r} - \mathbf{r}') \delta(t). \quad (3.33)$$

Clearly, fluctuations that are static on the scale of the delay time do not contribute to dephasing, so that in the limit of zero delay time, there is no dephasing (this corresponds to the conservation of the total particle number),

$$\mathcal{D}_{\eta=0}(\omega, q) = \frac{1}{Dq^2 - i\omega}, \quad (3.34)$$

and in the limit of infinite-delay time, the result for the UCF diffuson is recovered,

$$\mathcal{D}_{\eta=\infty} = \mathcal{D}^{12}. \quad (3.35)$$

Unlike for conductance-fluctuation diffuson (3.31), static approximation (3.3) cannot be directly used, since it assumes that the dynamics of the gauge field is the slowest scale of the system (only the time separation between two independent measurements is longer).

To account for *finite-delay* times η , we refine the static approximation by inspecting the diffuson analog of Eq. (3.12),

$$\begin{aligned}
\Delta S_\eta(t) &= \frac{1}{2} \lambda^2 e^2 \int_{-t}^t dt_1 \int_{-t}^t dt_2 \dot{r}_\alpha(t_1) \dot{r}_\beta(t_2) \\
&\times \{ \langle a_\alpha[\mathbf{r}_1, (t_1 + \eta/2)] a_\beta[\mathbf{r}_2, (t_2 + \eta/2)] \rangle \\
&- \langle a_\alpha[\mathbf{r}_1, (t_1 + \eta/2)] a_\beta[\mathbf{r}_2, (t_2 - \eta/2)] \rangle \\
&- \langle a_\alpha[\mathbf{r}_1, (t_1 - \eta/2)] a_\beta[\mathbf{r}_2, (t_2 + \eta/2)] \rangle \\
&+ \langle a_\alpha[\mathbf{r}_1, (t_1 - \eta/2)] a_\beta[\mathbf{r}_2, (t_2 - \eta/2)] \rangle \}.
\end{aligned} \tag{3.36}$$

The action ΔS_η of the delayed diffuson can be obtained from the action of the Cooperon ΔS by defining the effective correlator

$$\langle a_\alpha a_\beta \rangle_{\mathbf{k}, \epsilon}^{\text{diff}}(\eta) = \langle a_\alpha a_\beta \rangle_{\mathbf{k}, \epsilon} [1 - \cos \epsilon \eta], \tag{3.37}$$

where the factor in the brackets⁴⁷ arises from the combinations of the time arguments in Eq. (3.36). For the Cooperon in the static approximation, the factor corresponding to the brackets in Eq. (3.37) is simply 2 because in that case self-energy and vertex contributions equally *add*. In this context, it is important to note that applying static approximation (3.3) and taking the limit of infinite η in Eq. (3.36) do not commute. For the UCF diffuson, the correct procedure used in Sec. III B is to first send $\eta \rightarrow \infty$, which results in the vertex contributions dropping out. We also remind that for the same reason, at very long times $t \gg 1/T_0$, the static approximation is not applicable, and the Cooperon dephasing rate reduces to *half* the value given by Eq. (3.23) [see Eqs. (3.25) and (3.27)].

For the delayed diffuson, the cosine term in Eq. (3.37) effectively removes the fluctuations that are slow on the time scale η from the calculations for the conductance-fluctuation diffuson (Sec. III B): For short delay times $\eta \ll 1/T$, it results in an extra suppression factor $\frac{1}{2} \epsilon^2 \eta^2$. This suppression factor is due to the cancellation of self-energy and vertex terms imposed by particle number conservation.⁴⁷ For long delay times $\eta \gg 1/T$, the oscillating contribution drops out, which results in the long- η dephasing rate of the delayed diffuson being half the dephasing rate of the Cooperon in a *static* RMF [Eq. (3.23)].

The contribution of thermal gauge-field fluctuations relevant for dephasing of a diffusion with finite-delay time η can thus be written in analogy to Eq. (3.4) as

$$\langle a_\alpha a_\beta \rangle_{\mathbf{k}}^{\text{diff}}(\eta) = \int_{-T}^T \frac{d\epsilon}{2\pi} \langle a_\alpha a_\beta \rangle_{\mathbf{k}, \epsilon}^{\text{diff}}(\eta). \tag{3.38}$$

For $\eta \gg 1/T$, Eq. (3.38) can be approximated as

$$\begin{aligned}
\langle a_\alpha a_\beta \rangle_{\mathbf{k}}^{\text{diff}}(\eta) &= \int_{|\epsilon| > 1/\eta}^{|\epsilon| < T} \frac{d\epsilon}{2\pi} \langle a_\alpha a_\beta \rangle_{\mathbf{k}, \epsilon} \\
&= \frac{2T}{\pi \chi_0 k^2} \delta_{\alpha\beta}^\perp \left[\arctan T_k |\eta| - \arctan \frac{T_k}{T} \right] \\
&\approx \frac{2T}{\pi \chi_0 k^2} \delta_{\alpha\beta}^\perp \arctan T_k |\eta|, \quad T \gg T_0, |\eta| \gg 1/T,
\end{aligned} \tag{3.39}$$

where $T_k \equiv \chi_0 k^2 / \sigma_0 = k^2 l^2 T_0$. For short delay times $|\eta| \ll 1/T$, we find

$$\begin{aligned}
\langle a_\alpha a_\beta \rangle_{\mathbf{k}}^{\text{diff}}(\eta) &\approx \int_{-T}^T \frac{d\epsilon}{2\pi} \langle a_\alpha a_\beta \rangle_{\mathbf{k}, \epsilon} \frac{1}{2} \epsilon^2 \eta^2 \\
&= \frac{T \eta^2}{\pi \sigma_0} \left[T - T_k \arctan \frac{T}{T_k} \right] \delta_{\alpha\beta}^\perp \\
&\approx \begin{cases} \frac{T^2 \eta^2}{\pi \sigma_0} \delta_{\alpha\beta}^\perp, & T \gg T_k, |\eta| \ll 1/T \\ \frac{T^4 \eta^2}{3 \pi \sigma_0 T_k^2} \delta_{\alpha\beta}^\perp, & T \ll T_k, |\eta| \ll 1/T. \end{cases}
\end{aligned} \tag{3.40}$$

Using correlator (3.39) or (3.40) instead of Eq. (3.3) in Eq. (3.18), we can derive a dephasing action for the delayed diffuson which corresponds to the dephasing action [Eq. (3.21)] for the Cooperon. In contrast to the Cooperon dephasing in a static RMF, only gauge-field fluctuations that are *fast* on the scale η contribute. These fluctuations incoherently add up (instead of coherently for the static ones). The dephasing rate of the infinitely delayed diffuson is therefore half the dephasing rate of the Cooperon in a truly static RMF, and the same as that of a Cooperon for times $t \gg 1/T_0$, when the gauge field cannot be regarded as static.

Compared to the situation in Sec. III A, finite-delay times modify the low- k cutoff L_ω^{-1} in Eq. (3.20) in the following way: $L_\eta \equiv (\chi \eta / \sigma_0)^{1/2} = (T_0 \eta)^{1/2} l$ replaces L_ω if it is shorter, which modifies the cutoff of the logarithm. If η is so short that $L_\eta \approx l$, the logarithm collapses and the otherwise sub-leading term becomes the dominant one. We find the following dephasing action for $T_0 \ll T \ll T_1 / \lambda^2$:

$$\Delta S_\eta^{\text{eff}}(t) \approx \begin{cases} 3 \lambda^2 g T t \ln \frac{t}{\tau}, & |\eta| \gg g^2 t \\ 3 \lambda^2 g T t \ln(T_0 |\eta|), & 1/T_0 \ll |\eta| \ll g^2 t \\ \frac{6}{\pi} \lambda^2 g T t T_0 |\eta|, & 1/T \ll |\eta| \ll 1/T_0 \\ \frac{3}{\pi} \lambda^2 g T^2 t T_0 \eta^2, & |\eta| \ll 1/T. \end{cases} \tag{3.41}$$

The dephasing rates are defined by the condition $\Delta S_\eta^{\text{eff}}(t = \tau_\varphi) = 1$ and read for $T_0 \ll T \ll T_1 / \lambda^2$,

$$\frac{1}{\tau_\varphi(\eta)} \approx \begin{cases} 3 \lambda^2 g T \ln(T_0 \eta^*), & 1/T \ll 1/T_0 \ll |\eta| \\ \frac{6}{\pi} \lambda^2 g T T_0 |\eta|, & 1/T \ll |\eta| \ll 1/T_0 \\ \frac{3}{\pi} \lambda^2 g T^2 T_0 \eta^2, & |\eta| \ll 1/T \ll 1/T_0, \end{cases} \tag{3.42}$$

where

$$\eta^* = \min\{|\eta|, g/\lambda^2 T\}. \tag{3.43}$$

For later reference (to ensure that we may neglect dephasing in Sec. IV B), we also estimate the dephasing action for the case $T \ll T_0$. Then, in addition to the low- k cutoff, a high- k cutoff appears, such that $k \leq l_T^{-1} \equiv (T/T_0)^{1/2} l^{-1}$. This condition is stronger than the cutoff by the elastic mean free path at low temperatures, $T \lesssim T_0$ [see Eq. (3.26)]. As a result, we find the dephasing action

$$\Delta S_\eta^{\text{eff}}(t) \approx \begin{cases} 3\lambda^2 g T t \ln \frac{t}{\tau^*}, & |\eta| \gg g^2 t \\ 3\lambda^2 g T t \ln(T|\eta|), & 1/T \ll |\eta| \ll g^2 t \\ \frac{4}{\pi} \lambda^2 g T^3 \eta^2 t, & |\eta| \ll 1/T, \end{cases} \quad (3.44)$$

with $\tau^* = (T_0/T)\tau$. Equation (3.44) gives the following dephasing rates for $T \ll T_0$,

$$\frac{1}{\tau_\varphi(\eta)} \approx \begin{cases} 3\lambda^2 g T \ln(T\eta^*), & 1/T_0 \ll 1/T \ll |\eta| \\ \frac{4}{\pi} \lambda^2 g T^3 \eta^2, & |\eta| \ll 1/T. \end{cases} \quad (3.45)$$

It should be noted that in the long-time limit $t \rightarrow \infty$, the quasiclassical approximation (employed in the path-integral calculation) breaks down. This occurs at the time scale $t \gg t^* \sim E_F \eta \tau_\varphi(\eta)$, which, in particular, satisfies $t^* \gg \tau_\varphi(\eta)$ for any η . The reason for the breakdown is that the two quasiclassical trajectories can eliminate the delay (and therefore further suppression) by quantum “tunneling” (assuming nonclassical velocities during some time). This happens at the cost of an extra phase difference which is, however, smaller than the one for the delayed paths with classical velocities. As a result, for $t \gg t^*$, the diffuson is no longer decaying with increasing time t ; particle number conservation and the corresponding diffusion pole for small frequencies are restored in the long-time limit. However, the weight of the diffusion pole is exponentially small due to the suppression factor associated with the nonclassical pieces of the trajectories. The results of this paper are not affected by the breakdown of the quasiclassical approximation since all relevant time scales are shorter than t^* .

It is also worth mentioning that the virtual interaction processes renormalize the quasiclassical trajectories (velocity, diffusion constant). For the case of weak coupling considered above, these effects are negligible. However, they become important in the strong-coupling limit (see Sec. IV).

D. Diffuson dephasing: Two-loop localization correction

Since we have understood in Secs. III A–III C that dephasing of Cooperons and diffusons in the presence of a slowly fluctuating gauge field are mostly time-reversal breaking and ensemble-averaging effects, respectively, rather than true rates of loss of phase memory of the fermions, it is natural to ask if it is possible to avoid these effects and access the true dephasing rates. The diffuson contribution to the two-loop (second order in g) weak localization is sensitive to neither time-reversal breaking (since it contains no

Cooperons) nor ensemble averaging (since weak localization already is an ensemble-averaged quantity, corresponding to the “same measurement,” in contrast to the UCF diffusons). Therefore, the diffuson two-loop weak localization is not expected to be subject to the very high dephasing rates applicable to the Cooperons and the UCF diffusons. (It should be noted, however, that this two-loop correction to the conductivity is very hard to experimentally study, since it is insensitive to magnetic fields and much smaller than interaction corrections.)

The diffuson contribution to two-loop weak-localization correction $\delta\sigma_{\text{WL}}^D$ includes the structure^{36,47}

$$A_2 = \int_0^t dt' \langle \mathcal{D}_{t'-t}(\mathbf{r}, \mathbf{r}, t') \mathcal{D}_{t'}(\mathbf{r}, \mathbf{r}, t-t') \rangle, \quad (3.46)$$

with two delayed diffusons of type (3.33) along with a similar structure A_3 consisting of three delayed diffusons. As already seen in Eq. (3.33), a gauge field that does not change on the scale of the delay time drops out.^{19,47} Here, the delay times are given by the duration of the respective other path. It should be noted that anomalous sets of paths with one very small loop, which are not strongly suppressed because the short loop gives a short delay time of the other loop, drop out because of a cancellation of contribution (3.46) with a three-diffuson contribution.⁴⁷ As a result, relevant values of t and $t-t'$ in Eq. (3.46) are of the same order. To estimate the dephasing time associated with the two-loop correction, we may therefore self-consistently set $1/\tau_\varphi^D(\eta = \tau_\varphi^D) = 1/\eta$ in the respective delayed-diffuson dephasing rates [Eqs. (3.42) and (3.45)]. In the weak-coupling regime, $\lambda^2 g \ll 1$, the results are

$$\frac{1}{\tau_\varphi^D} \sim \begin{cases} \lambda^2 g T, & T \ll T_0/\lambda^2 g \\ \lambda(TT_1)^{1/2}, & T_0/\lambda^2 g \ll T \ll T_1/\lambda^2. \end{cases} \quad (3.47)$$

As expected, $1/\tau_\varphi^D$ is smaller than the Cooperon dephasing rate $1/\tau_\varphi$ as given by Eqs. (3.23), (3.25), and (3.27). This is at variance with the conventional Coulomb interaction, for which the diffuson dephasing rate in the second-loop weak-localization correction is of the same order⁴⁷ as the Cooperon dephasing rate.

In the strong-coupling regime, $\lambda^2 g \gg 1$, the second-loop diffuson dephasing rate becomes of the order of the temperature, owing to the interaction-induced renormalization of the paths contributing to the weak-localization correction (see the discussion in Sec. IV D). As mentioned in Sec. III A, for the half-filled lowest Landau level, the time-reversal symmetry is broken because of the strong magnetic field. In the context of composite fermions, this manifests itself in the way that also the static scalar impurities acquire a vector component due to screening. Therefore, weak localization is absent in the first order in $1/g$, and the two-loop diffuson contributions discussed here give the leading localization correction. This correction, along with the interaction correction at low temperatures which we will discuss in Sec. IV B, strongly indicates that the system of composite fermions interacting via a Chern–Simons gauge field is localized in the limit $T \rightarrow 0$.

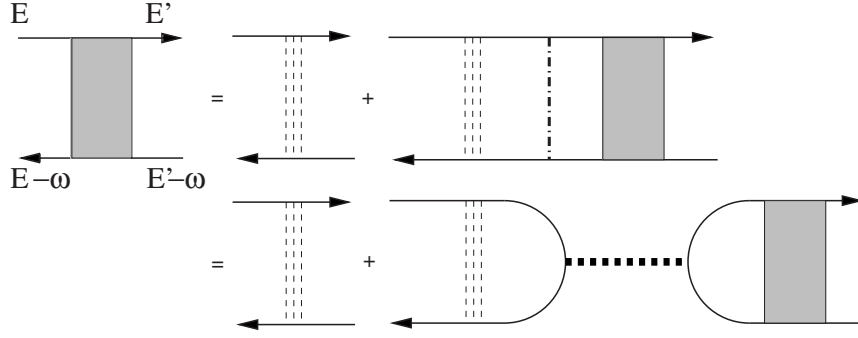


FIG. 8. The interaction-dressed diffuson described by Eq. (4.8). The impurity ladders here denote the “disconnected diffusons” $\tilde{\mathcal{D}}_\infty$ with only self-energy interaction lines included; the vertex interaction (dashed-dotted) line enters along with the additional diagrams from Fig. 2 which form the effective interaction \tilde{U} (thick dotted line).

IV. STRONG COUPLING: HARTREE CORRECTION AND DEPHASING

A. Diffuson self-energies

Let us now discuss the situation of strong coupling, $\lambda^2 g \gg 1$. Since the first-order result [Eq. (2.8)] is not a small correction then, it is necessary to take the interaction into account to all orders. We have to include both virtual (renormalization) processes, which are determined by the real part of the interaction propagator and real (dephasing) processes, which are determined by the imaginary part of the interaction propagator. For the conceptual framework of treatment of interaction effects in disordered systems, we refer the reader to Refs. 30, 31, 48, and 49.

The virtual processes are taken into account by inserting the self-energies (diagrammatically calculated in Appendix D) into the delayed diffusons. The treatment of the dephasing processes by using the path-integral method as discussed in Sec. III C is complemented by the diagrammatic calculation of the dephasing-induced self-energy of the delayed diffusons.

We first calculate the self-energies in the first order in the effective interaction for $\lambda \ll 1$. As we are going to show below, neither Hartree conductivity correction nor the dephasing rate depends on λ already for $\lambda^2 \gg 1/g$. This allows us to evaluate these quantities in the relevant case of $\lambda=1$ using the results derived for $1/g \ll \lambda^2 \ll 1$ up to the numerical prefactors (stemming from the contribution of higher-order interaction terms in the interaction blocks). The situation is somewhat similar to the conventional Coulomb interaction case, where the Hartree ladder in the triplet channel depends on the Fermi-liquid constants,²⁵ which makes it impossible to analytically calculate the numerical coefficients in the conductivity corrections for $r_s \gtrsim 1$ (where r_s , an analog of λ here, is the standard gas parameter) starting from the microscopic theory.

It is important that higher-order-in- λ contributions do not lead to any further singularities, in contrast to the clean situation.² The expansion of the effective interaction in λ is regular in the present disordered case, since disorder cures the infrared singularities arising in the clean² theory. The additional (as compared to the clean situation) characteristic energy scales are introduced by disorder: T_0 and $1/\tau$. On

scales longer than the mean free path, the dynamics of the system is diffusive. In the first-order interaction terms, the infrared singularity at low momenta \mathbf{k} transferred through the gauge-interaction lines is cut off by additional diagrams involving impurity ladders (see Fig. 2), as discussed in Sec. II. Furthermore, a resummation of the higher-order interaction terms in the fermionic self-energies is not needed in the diffusive regime, i.e., as long as the first-order self-energy does not exceed $1/\tau$.

The peculiarity of the interaction block $\tilde{U}(q)$ (thick dotted line in Fig. 2) is that its magnitude is very large ($\propto g$) in a narrow window of small momentum transfers $q \lesssim 1/l$ [see Eq. (2.5)]. A similar situation takes place in a normal metal with the Coulomb interaction, where the bare interaction is singular ($\propto 1/q$) and hence can be arbitrarily strong in the limit of small q . The screening of the Coulomb interaction in normal metals is described by the RPA and results in a much less singular effective interaction [Eq. (2.6)]. Therefore, in analogy to the standard situation, we first consider the resummation of an infinite number of higher-order virtual processes. This can be described by an integral equation for the diffuson, which sums up blocks of the (real part of the) effective interaction in an RPA-inspired way, yielding a renormalized diffuson. The dephasing will be included later on in Sec. IV A 1.

As a result of the resummation, we will find the renormalized one-loop Hartree correction to the conductivity. It still contains only one Hartree fermionic bubble, as the perturbative correction in Sec. II, so that all diffusons form a single loop. Another source of higher-order Hartree corrections is provided by higher-loop diagrams with many Hartree fermionic bubbles attached to the main “conductivity bubble” (before disorder averaging, they correspond to diagrams with many tadpoles). These diagrams are relevant in the situation when the one-loop result exceeds the Drude conductivity. An efficient way of resummation of such diagrams (a certain type of self-consistent approximation) has been proposed in Ref. 50 in the context of the tunneling density of states in superconductors. However, as we are going to show, in the present problem, the renormalization of diffusons prevents the one-loop Hartree correction from being larger than the Drude conductivity. Therefore, the additional resummation⁵⁰ of higher-loop diagrams is not needed.

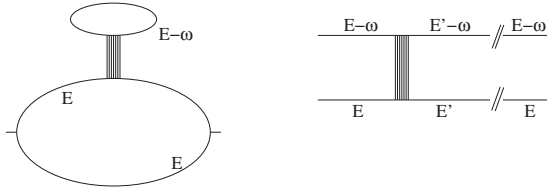


FIG. 9. The energies of the renormalized diffusons in the Hartree diagrams satisfy $E, E' \lesssim T$ and $\omega \gtrsim T$.

In the presence of interaction, the energies of the (retarded and advances) Green's functions forming the diffuson may change due to the vertex interaction lines transferring finite energy from the upper to the lower fermionic line. Therefore, the interaction-dressed diffuson not only depends on the difference ω between the energies of two (retarded and advances) Green's functions but also on the incoming and outgoing energies, E and E' (for definiteness, these are the energies of the retarded Green's functions). The diffuson

$\tilde{\mathcal{D}}(E, E'; \omega, q)$ dressed by vertex and self-energy gauge-field interaction lines satisfies the equation (see Figs. 8 and 9)

$$\begin{aligned} \tilde{\mathcal{D}}(E, E'; \omega, q) &= \delta(E - E') \mathcal{D}_0(\omega, q) + 2\pi\nu \mathcal{D}_0(\omega, q) \\ &\times \int_{E-\omega}^E \frac{d\epsilon}{2\pi} (-i) \text{Re} \tilde{U}(\epsilon) [\tilde{\mathcal{D}}(E - \epsilon, E'; \omega, q) \\ &- \tilde{\mathcal{D}}(E, E'; \omega, q)]. \end{aligned} \quad (4.1)$$

Here, we set $T=0$ for simplicity. At finite temperature, a standard combination of thermal factors $\tanh[(E-\epsilon)/2T] - \tanh[(E-\omega-\epsilon)/2T]$ appears which in effect softens the limits of ϵ integration on the scale of T (for $\omega \gtrsim T$, this effect is inessential). The first term in brackets under the integral in Eq. (4.1) is the vertex interaction part (see Fig. 2), the second one is the self-energy part (see Fig. 10), and

$$\mathcal{D}_0 = \frac{1}{Dq^2 - i\omega} \quad (4.2)$$

is the bare (noninteracting) diffuson. The effective interaction $\tilde{U}(\epsilon)$ corresponds to the interaction block in Fig. 2 in the vertex part; in the self-energy part, the same structure arises from diagrams in Fig. 10. The real part of $\tilde{U}(\epsilon)$ involved in the renormalized diffuson [Eq. (4.1)] reads (see Appendix D)

$$\text{Re } \tilde{U}(\epsilon) \approx \frac{3\lambda^2 g}{\pi\nu} \begin{cases} \ln \frac{1}{q^2 l^2}, & |\epsilon| \ll T_0 q^2 l^2 \\ \ln \frac{T_0}{|\epsilon|}, & T_0 q^2 l^2 \ll |\epsilon| \ll T_0 \\ \frac{4\pi}{3} \left(\frac{T_0}{2|\epsilon|} \right)^{1/3}, & |\epsilon| \gtrsim T_0. \end{cases} \quad (4.3)$$

Here, it is worth recalling that we are dealing with spinless (spin-polarized) fermions (which is, in particular, the case for the composite fermions at the lowest Landau level). At variance with the singlet channel in the standard case, the Hartree gauge-field ladder is not affected by the possible insertion of gauge-field "exchange" parts. The reason is that, due to the vector character of the vertices, no disorder lines (and hence extra diffusons) may separate the exchange interaction line from the adjacent Hartree interaction lines. Therefore, inserting an exchange interaction line gives a result that is smaller by a factor of the order of $q^2 l^2 \ll 1$.

The range of energy integration for the single self-energy block is $[E-\omega, E]$ and hence depends on the total energy of the diffuson. The full ladder is part of a Hartree diagram, which features $E \lesssim T$ (the energy in the conductivity bubble is restricted by the thermal factors from the Kubo formula), but $E-\omega$ (energies of the attached bubble) are unbounded from below and characterized by $\omega \gtrsim T$, owing to the standard thermal factor $(\partial/\partial\omega)[\omega \coth(\omega/2T)]$ in the interaction correction to the conductivity (see Fig. 9). It is convenient to introduce a "disconnected" diffuson $\tilde{\mathcal{D}}_\infty \delta(E-E')$ dressed only by self-energy lines,

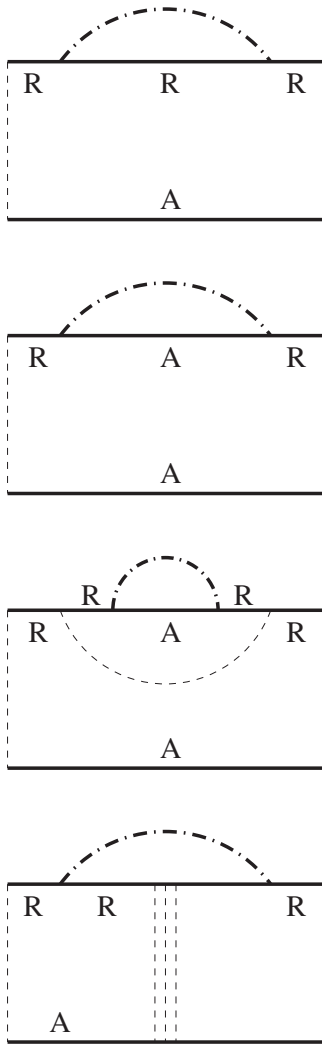


FIG. 10. Self-energy counterparts to the vertex interaction (Fig. 2), resulting in the diffuson self-energy [Eq. (4.15)]. In addition to the diagrams shown, equivalent possibilities to insert self-energy lines into the advanced Green's function exist. The detailed calculation can be found in Appendix D.

$$\begin{aligned}\tilde{\mathcal{D}}_\infty &= \frac{\mathcal{D}_0}{1 + 2\pi\nu\mathcal{D}_0 \int_{E-\omega}^E \frac{d\epsilon}{2\pi} (-i)\text{Re} \tilde{U}(\epsilon)} \\ &= \frac{1}{Dq^2 - i\omega - i\nu \int_{E-\omega}^E d\epsilon \text{Re} \tilde{U}(\epsilon)}.\end{aligned}\quad (4.4)$$

For the disconnected diffuson, the fact that we are interested in $\omega \gtrsim T \gtrsim E$ allows us to neglect E in the limits of the ϵ -integration.

In the full diffuson [Eq. (4.1)] including the vertex lines, the energy is no longer conserved along the fermionic Green's functions, so that the E dependence of the integration limits becomes important. Although we are still interested in $\omega \gg E$, the integral equation for the full diffuson involves propagators with $E \sim \omega$ at the intermediate steps of the ladder, thus making the exact analytical solution of Eq. (4.1) impossible. In what follows, we will simplify the equation for the diffuson, by neglecting the energy dependence of the integration limits.

This approximation, which is closely related to that of Ref. 49, while giving the correct T dependence of the Hartree conductivity correction, does not allow us to find the exact numerical prefactor at low temperatures. This prefactor, however, is not too important since the low- T dependence of the total conductivity correction will be dominated by the exchange contribution, as we will show below. In this regime ($T \ll T_0$), the relevant delay times are short, $\eta \lesssim 1/\omega$, and fluctuate within the window ω^{-1} from one step of the diffuson ladder to another. At higher temperatures, when the conductivity correction is dominated by long $\eta \gg 1/\omega$, the diffuson delay time is well defined and our approximation is controlled by the parameter $\omega/T \gg 1$ [see, e.g., Eq. (4.38) below, which is governed by $T < \omega < T_0$].

Within the approximation described above, Eq. (4.1) is replaced by the equation for the diffuson which now depends only on the difference of the two energies $E - E'$, corresponding to a fixed delay time η in the time domain (to simplify notation, we do not write the diffuson frequency ω and momentum q ; we also assume $T=0$ here),

$$\begin{aligned}\tilde{\mathcal{D}}(E - E') &= \mathcal{D}_0 \delta(E - E') + 2\pi\nu\mathcal{D}_0 \int_{-\omega}^0 \frac{d\epsilon}{2\pi} (-i)\text{Re} \tilde{U}(\epsilon) \\ &\quad \times [\tilde{\mathcal{D}}(E - \epsilon - E') - \tilde{\mathcal{D}}(E - E')].\end{aligned}\quad (4.5)$$

It can be solved by Fourier transformation to the (delay) time domain with respect to $E - E'$,

$$\tilde{\mathcal{D}}_\eta(q, \omega) = \frac{1}{Dq^2 - i\omega - i\Sigma_\eta^Z}, \quad (4.6)$$

with

$$\Sigma_\eta^Z = 2\pi\nu \int_{-\omega}^0 \frac{d\epsilon}{2\pi} \text{Re} \tilde{U}(\epsilon) [1 - \cos \epsilon\eta]. \quad (4.7)$$

Equation (4.5) for the fully renormalized diffuson can be rewritten as

$$\begin{aligned}\tilde{\mathcal{D}}(E - E') &= \tilde{\mathcal{D}}_\infty \delta(E - E') + 2\pi\tilde{\mathcal{D}}_\infty \\ &\quad \times \int_{-\omega}^0 \frac{d\epsilon}{2\pi} (-i)\text{Re} \tilde{U}(\epsilon) \tilde{\mathcal{D}}(E + \epsilon - E'),\end{aligned}\quad (4.8)$$

in terms of the disconnected diffuson $\tilde{\mathcal{D}}_\infty$ given by Eq. (4.4), with E neglected in the limits of the ϵ integration.

Let us discuss how the delayed diffusons $\tilde{\mathcal{D}}_\eta$ enter the Hartree correction. For the lowest-order Hartree diagrams in Fig. 1, the condition of zero energy transfer through the single interaction line can be rewritten by the substitution,

$$(-i)\text{Re} \tilde{U}(q, \epsilon=0)\mathcal{B} \rightarrow \int d\eta (-i)u(\eta)\mathcal{B}(\eta), \quad (4.9)$$

where $u(\eta)$ is the Fourier transform of the real part $\text{Re} \tilde{U}(\epsilon)$ [Eqs. (D4) and (4.3)] of the effective interaction $\tilde{U}(\epsilon)$,

$$u(\eta) \approx \begin{cases} \frac{3\lambda^2 g}{2\pi\nu} \gamma_1 T_0^{1/3} \eta^{-2/3}, & 0 < |\eta| \leq \frac{1}{T_0} \\ \frac{3\lambda^2 g}{2\pi\nu|\eta|}, & \frac{1}{T_0} \leq |\eta| \leq \frac{1}{q^2 l^2 T_0}, \end{cases}\quad (4.10)$$

[with $\gamma_1 = \Gamma(5/3)/2^{1/3}$, where $\Gamma(x)$ is the gamma function] and \mathcal{B} is the fermionic part of the diagram.

Using the diagrams of Figs. 1(a) and 1(b), we can rewrite the first-order Hartree correction in terms of the delayed interaction $u(\eta)$,

$$\begin{aligned}\delta\sigma^H &\approx \sigma_0 \text{Re} \int_{-\infty}^{\infty} \frac{d\omega}{2\pi} \frac{\partial}{\partial\omega} \left[\omega \coth \frac{\omega}{2T} \right] \int_{-\infty}^{\infty} d\eta \int (dq) \mathcal{D}_0(\omega, q) \\ &\quad \times (-i)u(\eta)\mathcal{D}_0(\omega, q).\end{aligned}\quad (4.11)$$

In this first-order correction, the fermionic part \mathcal{B} does not depend on the delay time. Correction (4.11) is dominated by long delay times $\eta \gg 1/T_0$, with the integration over η yielding the logarithm in Eq. (2.5), which leads to the $\ln^2 T$ temperature dependence [Eq. (2.8)] found in Sec. II A.

For a more refined treatment including higher-order interaction terms, it is necessary to keep track of the energy arguments E and E' of the diffusons. Then, the Hartree correction to the conductivity can be evaluated using the diagrams that now should contain diffusons renormalized by additional self-energy and vertex interaction lines. This implies that the fermionic part \mathcal{B} of the diagrams becomes η dependent, since there is a time difference between the Hartree bubble and the main ‘‘conductivity fermionic loop,’’ owing to the slow dynamics of gauge fields.

In technical terms, in the first-order interaction diagrams in Fig. 3, each effective interaction line \tilde{U} is dressed from both sides by impurity ladders [see, e.g., Eq. (4.11)]. In higher-order diagrams, the product of the effective interaction \tilde{U} with the two adjacent bare diffusons is replaced by a single fully dressed diffuson $\tilde{\mathcal{D}}_\eta$ minus the completely disconnected contribution $\tilde{\mathcal{D}}_\infty$ (with only self-energy interaction

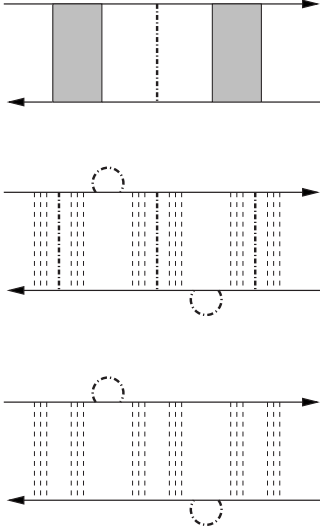


FIG. 11. In the presence of self-energy and vertex interactions dressing the diffusons, the effective interaction block \tilde{U} together with the two adjacent dressed diffusons can be more conveniently considered as one diffuson renormalized by the self-energy and vertex interaction lines, and the disconnected part subtracted to ensure the Hartree structure of at least one interaction line connecting the fermionic bubbles.

lines but no vertex interaction line) (see Fig. 11),

$$[\mathcal{D}_0(-i)\text{Re}\{\tilde{U}\}\mathcal{D}_0]_\eta \rightarrow \frac{1}{2\pi\nu}[\tilde{\mathcal{D}}_\eta - \tilde{\mathcal{D}}_\infty]. \quad (4.12)$$

The subtraction of the disconnected part ensures the Hartree structure of the contribution under consideration: at least one vertex interaction line connects the two fermionic bubbles. This formula will be used in Sec. IV B for $T \ll T_0$, when dephasing can be neglected.

Transforming the fully dressed diffuson [Eq. (4.8)] to delay time space and subtracting the disconnected part $\tilde{\mathcal{D}}_\infty$, we find

$$\frac{1}{2\pi\nu}[\tilde{\mathcal{D}}_\eta - \tilde{\mathcal{D}}_\infty] = \tilde{\mathcal{D}}_\infty(-i)u(\eta)\tilde{\mathcal{D}}_\eta. \quad (4.13)$$

Since $\text{Im}\tilde{U}$ enters the dephasing self-energy Σ_η^φ , only $\text{Re}\tilde{U}$ should be kept for the renormalization. Equation (4.13) explicitly singles out a Hartree (renormalization) interaction line. The dephasing is then included into the diffusons on the right-hand side of Eq. (4.13). This expression will be used in Sec. IV C for calculation of the Hartree conductivity correction at intermediate temperatures $T_0 \ll T \ll T_1$, when dephasing may be strong compared to the renormalization effects.

1. Disconnected diffuson

Now, we include the dephasing into the delayed diffuson. We start with the simpler case of a disconnected diffuson (infinite delay time), which has already appeared in Sec. III B as the UCF diffuson. As discussed in Appendix D, the disconnected diffuson $\tilde{\mathcal{D}}_\infty$ has the form

$$\tilde{\mathcal{D}}_\infty = \frac{1}{Dq^2 - i\omega - i\Sigma_\infty^Z + \Sigma_\infty^\varphi}, \quad (4.14)$$

with the renormalization part of the self-energy

$$\Sigma_\infty^Z = \frac{3\lambda^2}{2\pi}g\omega f_Z\left(\frac{T_0}{\omega}\right), \quad (4.15)$$

where $f_Z(x)$ is a slowly varying function

$$f_Z(x) \approx \begin{cases} \ln x + 1, & x \gg 1 \\ \pi(4x)^{1/3}, & x \ll 1. \end{cases} \quad (4.16)$$

The high- ω behavior of Eq. (4.15) is reminiscent of the ballistic behavior in a clean system.⁶ The self-energy Σ_∞^Z can be cast in the form

$$\Sigma_\infty^Z = \omega[Z(\omega) - 1], \quad (4.17)$$

where $Z(\omega) = 1 + (3\lambda^2 g/2\pi)f_Z(T_0/\omega)$ represents an effective Z factor renormalizing the frequency, hence the superscript Z .

The dephasing-induced part Σ_∞^φ of the self-energy of the disconnected diffuson is also given by diagrams in Fig. 10, now with the imaginary part of the interaction propagator and the appropriate thermal factor [see Eq. (4.18)]. For $\omega \ll T$, it can also be obtained by the path-integral calculation of Sec. III C, using the classical (thermal) part of the interaction propagator for $\epsilon \ll T$, since for $\omega, E \ll T$, the high-energy transfers with $|\epsilon| > T$ are suppressed by the standard inelastic thermal factor $\coth(\epsilon/2T) - \tanh(\epsilon/2T)$. Then, $\Sigma_\infty^\varphi \propto \lambda^2 g T$ is given by Eqs. (3.42) and (3.45) with $\eta = \infty$ and the logarithmic factor (see Sec. IV D below) modified by the renormalization processes.

For $\omega \gtrsim T$ and $E \lesssim T$, which is the range relevant for the Hartree correction to the conductivity, the full inelastic thermal factor^{24,30,49,51}

$$\begin{aligned} & \coth\frac{\epsilon}{2T} + \frac{1}{2} \left[\tanh\frac{E-\epsilon}{2T} + \tanh\frac{E-\omega-\epsilon}{2T} \right] \\ & \simeq \coth\frac{\epsilon}{2T} - \frac{1}{2} \left[\tanh\frac{\epsilon}{2T} + \tanh\frac{\omega+\epsilon}{2T} \right] \\ & \simeq \begin{cases} 0, & \epsilon \gg T \\ 2T/\epsilon, & |\epsilon| < T \\ -1, & -\omega \ll \epsilon \ll -T \\ 0, & \epsilon \ll -\omega \end{cases} \end{aligned} \quad (4.18)$$

allows also for real inelastic processes with energy transfers $-\omega < \epsilon < -T$. Thus, in addition to the standard range $|\epsilon| < T$ where the thermal factor is classical, $2T/\epsilon$, we have a contribution described by the quantum factor -1 (the phase space available for inelastic scattering is then determined by ω rather than by temperature). It is convenient to separate the thermal ($\Sigma_\infty^{\varphi,T}$) and frequency-induced ($\Sigma_\infty^{\varphi,\omega}$) contributions to the dephasing self-energy,

$$\Sigma_\infty^\varphi = \Sigma_\infty^{\varphi,T} + \Sigma_\infty^{\varphi,\omega}. \quad (4.19)$$

The thermal contribution can be still evaluated by the path-integral method and is given by Eqs. (3.42) and (3.45)

with the logarithmic factor determined by the diffuson momenta q through the infrared cutoff established by the gauge invariance

$$\Sigma_{\infty}^{\varphi,T} = 3\lambda^2 g T \begin{cases} \ln\left(\frac{1}{q^2 l^2}\right), & T \gg T_0 \\ \ln\left(\frac{T}{T_0 q^2 l^2}\right), & T \ll T_0. \end{cases} \quad (4.20)$$

The same result is diagrammatically obtained along the lines described in Appendix D.

One sees that the thermal contribution to the dephasing is proportional to the conductance and temperature, $\Sigma_{\infty}^{\varphi,T} \propto \lambda^2 g T$. In the strong-coupling regime, $\lambda^2 g \gg 1$, the thermal-dephasing part of the diffuson self-energy exceeds T . This result for the disconnected diffuson self-energy agrees with the path-integral calculation of the Cooperon and UCF-diffuson dephasing rate [Eqs. (3.23), (3.25), and (3.27)]: the path integral automatically chooses characteristic values of q in Eq. (4.20).

The frequency-induced dephasing self-energy is similar to the renormalization part Σ_{∞}^Z : at high frequencies $\omega \gg T_0$, it is also determined by the ballistic energy and/or momenta transfers,

$$\Sigma_{\infty}^{\varphi,\omega} = \lambda^2 g \omega f_{\varphi}\left(\frac{T_0}{\omega}\right), \quad (4.21)$$

with

$$f_{\varphi}(x) \sim \begin{cases} 1, & x \gg 1 \\ x^{1/3}, & x \ll 1. \end{cases} \quad (4.22)$$

The high-frequency ($\omega \gg T_0$) asymptotics of Eq. (4.21), $\Sigma_{\infty}^{\varphi,\omega} \propto \omega^{2/3}$, is, in fact, determined by the imaginary part of the self-energy of a single particle Green's function and agrees with the result of Ref. 6. However, in contrast to the clean case, there is no need in resummation of the higher-order interaction terms (for not too high $\omega < T_{3/2}$), since disorder generates a larger self-energy $i/2\tau$ in the Green's function.

2. Fully dressed delayed diffuson

The fully dressed diffusion $\tilde{\mathcal{D}}_{\eta}$ is characterized by a cancellation between self-energy and vertex lines, which is complete at zero delay time

$$\tilde{\mathcal{D}}_{\eta=0}(\omega, q) = \mathcal{D}_0(\omega, q) \quad (4.23)$$

and partial at finite delay time

$$\tilde{\mathcal{D}}_{\eta} = \frac{1}{Dq^2 - i\omega - i\Sigma_{\eta}^Z + \Sigma_{\eta}^{\varphi}}. \quad (4.24)$$

The renormalization part Σ_{η}^Z of the self-energy (see Fig. 10) is at low frequencies $\omega \ll T_0$ given by

$$\Sigma_{\eta}^Z = \frac{3\lambda^2}{2\pi} g \omega \left[\ln \frac{T_0}{\omega} \left(1 - \frac{\sin \omega \eta}{\omega \eta} \right) + 1 - \frac{\text{Si}(\omega \eta)}{\omega \eta} \right], \quad \omega \ll T_0, \quad (4.25)$$

where $\text{Si}(x)$ is the integral sine function. At high frequencies $\omega \gg T_0$, the renormalization part of the self-energy reads

$$\Sigma_{\eta}^Z = \begin{cases} \mathcal{O}(1) \lambda^2 g \omega (\omega \eta)^2 \left(\frac{T_0}{\omega}\right)^{1/3}, & \eta \ll 1/\omega \ll 1/T_0 \\ \Sigma_{\infty}^Z - 3\lambda^2 g T_0 \gamma_1(T_0 \eta)^{-2/3}, & 1/\omega \ll \eta \ll 1/T_0 \\ \Sigma_{\infty}^Z - 3\lambda^2 g / \eta, & 1/\omega \ll 1/T_0 \ll \eta. \end{cases} \quad (4.26)$$

The dephasing part of the self-energy can be evaluated in a similar way. Below, we present only the leading terms in the relevant range of frequencies $\omega \gg T$. At low temperatures $T \ll T_0$, the dephasing part Σ_{η}^{φ} of the self-energy is given by the frequency-induced part

$$\Sigma_{\eta}^{\varphi} \sim \begin{cases} \lambda^2 g \omega (\omega \eta)^2, & \eta \ll 1/\omega \\ \lambda^2 g \omega, & \eta \gg 1/\omega \end{cases} \quad (4.27)$$

for $T \ll \omega \ll T_0$. For higher frequencies $T \ll T_0 \ll \omega$, we get

$$\Sigma_{\eta}^{\varphi} \sim \begin{cases} \lambda^2 g \omega^{2/3} T_0^{1/3} (\omega \eta)^2, & \eta \ll 1/\omega \\ \Sigma_{\infty}^{\varphi,\omega}, & 1/\omega \ll \eta \ll 1/T \\ 3\lambda^2 g T \ln(T \eta) + \Sigma_{\infty}^{\varphi,\omega}, & 1/T \ll \eta \ll 1/T_0 q^2 l^2 \\ \Sigma_{\infty}^{\varphi,T} + \Sigma_{\infty}^{\varphi,\omega}, & \eta \gg 1/T_0 q^2 l^2 \end{cases}, \quad (4.28)$$

which now features the competition between the thermal and frequency-induced contributions at long η . Finally, at temperatures $T \gg T_0$, we find a similar result

$$\Sigma_{\eta}^{\varphi} \sim \begin{cases} \lambda^2 g \omega^{2/3} T_0^{1/3} (\omega \eta)^2, & \eta \ll 1/\omega \\ \Sigma_{\infty}^{\varphi,\omega}, & 1/\omega \ll \eta \ll 1/T_0 \\ 3\lambda^2 g T \ln(T_0 \eta) + \Sigma_{\infty}^{\varphi,\omega}, & 1/T_0 \ll \eta \ll 1/T_0 q^2 l^2 \\ \Sigma_{\infty}^{\varphi,T} + \Sigma_{\infty}^{\varphi,\omega}, & \eta \gg 1/T_0 q^2 l^2. \end{cases} \quad (4.29)$$

In the limit $\omega \ll T$, the dephasing part of the self-energy just reduces to the dephasing rate calculated using path integral in Sec. III C.

In the strong-coupling regime, when $\Sigma_{\infty}^Z \approx \omega Z(\omega) \gg \omega$, the integration over the diffuson momentum q in the Hartree conductivity correction is dominated by

$$Dq^2 \sim \max\{\Sigma^Z, \Sigma^{\varphi,\omega}, \Sigma^{\varphi,T}\}. \quad (4.30)$$

One can see from Eqs. (4.15), (4.21), and (4.22) that $\Sigma^{\varphi,\omega} \lesssim \Sigma^Z$ for any frequency: at $\omega \ll T_0$, there is an extra logarithmic factor in Σ^Z , while at $\omega \gg T_0$, the two quantities are of the same order. Therefore, in what follows, we neglect $\Sigma^{\varphi,\omega}$ for simplicity: its inclusion may only change the numerical coefficients in the results for the Hartree conductivity correction, which are anyway beyond the accuracy of the present approach.

On the other hand, the relation between $\Sigma^{\varphi,T}$ and Σ^Z depends on the frequency and temperature. At low tempera-

tures, inelastic scattering is suppressed. As a result, at $T \ll T_0$, we have $\Sigma^Z \gg \Sigma^{\varphi,T}$ for all relevant frequencies $\omega \gg T$. For $T \gg T_0$, the thermal dephasing dominates in the range of sufficiently low frequencies, $T \ll \omega \ll T(T/T_0)^{1/2}$, while the Z-factor renormalization wins at higher frequencies, $\omega \gg T(T/T_0)^{1/2}$. The self-energy part due to the thermal dephasing can always be evaluated using the path-integral approach developed in Sec. III C.

The diffusion approximation breaks down at high frequencies, when the self-energy of the disconnected diffuson becomes comparable to the elastic scattering rate $1/\tau$. The dephasing part $\Sigma^{\varphi,T}$ restricts our subsequent consideration at $\lambda=1$ to sufficiently low temperatures $T \ll T_1$ since $\Sigma_{\infty}^{\varphi,T}(T \sim T_1) \sim 1/\tau$. The Z factor poses the restriction on the frequency domain for diffusive dynamics, $\omega < 1/g^{1/2}\tau \equiv T_{3/2}$, since $\Sigma_{\infty}^Z(\omega \sim T_{3/2}) \sim 1/\tau$. We only consider the diffusive regime and hence restrict ourselves to the case $T < T_1$. We are now in the position to calculate the Hartree conductivity correction using the above results for the delayed-diffuson self-energies.

B. Low temperatures, $T \ll T_0$: Strong renormalization by self-energies

We start with the case of low temperatures, $T \ll T_0$. In this situation, the dephasing part of the self-energy Σ^{φ} [Eq. (4.19)] is smaller than the renormalization self-energy Σ^Z [Eq. (4.26)] for all ω and η and may be neglected. In Sec. IV C, we consider the situation $T \gg T_0$, where this is not the case and both renormalization and dephasing should be retained. In both temperature ranges, we calculate the Hartree correction in the realistic case $\lambda=1$.

We use the generalization of diagrams (a) and (b) with fully dressed diffusons, as described by Eq. (4.9). The result consists of a low-frequency contribution and a high-frequency contribution, with the low-frequency contribution given by

$$\delta\sigma_{\omega < T_0}^H = \frac{\sigma_0}{2\pi\nu} \int_{-T_0}^{T_0} \frac{d\omega}{2\pi} \frac{\partial}{\partial\omega} \left[\omega \coth \frac{\omega}{2T} \right] \times \int_{-\infty}^{\infty} d\eta \int (dq) [\tilde{\mathcal{D}}_{\eta} - \tilde{\mathcal{D}}_{\infty}]. \quad (4.31)$$

The details of the calculation of the low-temperature Hartree correction are presented in Appendix E. The result reads

$$\delta\sigma_{\omega < T_0}^H = \frac{e^2}{2\pi} \left[\frac{c_1}{2\pi^2} \ln \frac{T_0}{T} + \frac{1}{4\pi} \ln g \ln \left(\ln \frac{T_0}{T} + 1 \right) \right]. \quad (4.32)$$

The value of the constant given by a dimensionless integral [Eq. (E4)] is $c_1 \approx 5$. The strong renormalization of the frequency ω by a factor that is of order g at $T \ll T_0$ results in the prefactor of the $\ln(T_0/T)$ term in Eq. (4.32) being of order unity rather than of order g .

Here, at the low temperatures $T \ll T_0$ under consideration, the contribution of high frequencies $\omega \gg T_0$ saturates to a constant (again dephasing is unimportant compared to the self-energy),

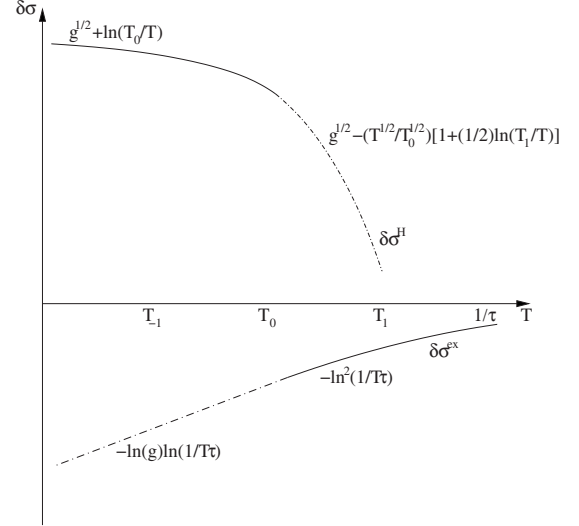


FIG. 12. Schematic plot of the Hartree correction to the conductivity, $\delta\sigma^H(T)$ for $\lambda=1$, in the different ranges of temperatures (log T scale). The solid and dotted-dashed lines of $\delta\sigma^H$ are described by the sum of Eqs. (4.32) and (4.33) and by Eq. (4.39), respectively. The exchange contribution (Ref. 17) $\delta\sigma^{\text{ex}}$ is shown for comparison. Due to the high dephasing rates of delayed diffusons, the Hartree contribution can be calculated within the diffusive approximation only at temperatures below T_1 . At low temperatures $T < T_0$, the exchange contribution overcompensates the T -dependent part of the Hartree contribution, so that the total correction becomes localizing, $d\sigma/dT > 0$.

$$\delta\sigma_{\omega > T_0}^H = \mathcal{O}(1)e^2 \left[g^{1/2} - \frac{1}{2} \ln g \right], \quad T \ll T_0, \quad (4.33)$$

see also Eq. (4.39) below. The coefficient depends on details of the high-frequency cutoff, which we do not attempt to calculate here.

Thus, the temperature-dependent part of the Hartree correction at very low temperatures is given by Eq. (4.32),

$$\delta\sigma^H(T) = \frac{e^2}{4\pi^3} c_1 \ln \frac{T_0}{T}, \quad T \ll T_{-1}. \quad (4.34)$$

Due to the renormalization of the diffusons by the large self-energies, the coefficient of the low-temperature Hartree correction [Eq. (4.34)] is of order unity rather than of order g , in contrast to what could be expected from the perturbative result [Eq. (2.8)] taken at $\lambda=1$. As a result, the temperature dependence of the Hartree correction is overcompensated at low temperatures $T < T_0$ by the negative exchange correction,¹⁷ which carries a coefficient of order $\ln g$ (see Fig. 12). It should be emphasized that in contrast to the Hartree contribution, the exchange correction involves only true diffusons \mathcal{D}_0 (zero delay time) which are affected neither by dephasing nor by renormalization.

At higher temperatures, $T \gg T_0$, dephasing and renormalization effects are of similar importance. This situation is considered in Sec. IV C below. We remind that at high $T \gg T_1$, the diffusion approximation breaks down due to the strong dephasing ($L_{\varphi} \ll l$), so that we restrict ourselves to intermediate-temperature range, $T_0 \ll T \ll T_1$.

C. Interplay of renormalization and dephasing at intermediate temperatures, $T_0 \ll T \ll T_1$

Using the results of Sec. III C for self-energies of delayed diffusons, we will now construct a scheme to treat the interaction to all orders, while ensuring the Hartree structure of the calculated contributions also in the presence of dephasing by means of Eq. (4.13). The Hartree correction at $T_0 \ll T \ll T_1$ can be then written as

$$\delta\sigma^H = \sigma_0 \int_{-T_{3/2}}^{T_{3/2}} \frac{d\omega}{2\pi} \frac{\partial}{\partial\omega} \left[\omega \coth \frac{\omega}{2T} \right] \text{Re} \int_{-\infty}^{\infty} d\eta \times \int (dq) \tilde{D}_\infty(-i) u(\eta) \tilde{D}_\eta. \quad (4.35)$$

The dephasing self-energy Σ_∞^φ in one of the two diffusons ensures that the contribution from short delay times $\eta \lesssim 1/T_0$ is subleading, so that the main contribution is given by

$$\delta\sigma^H \approx 4\sigma_0 \int_0^{T_{3/2}} \frac{d\omega}{2\pi} \frac{\partial}{\partial\omega} \left[\omega \coth \frac{\omega}{2T} \right] \text{Re} \int_{1/T_0}^{\infty} d\eta \times \int (dq) \tilde{D}_\infty(-i) u(\eta) \tilde{D}_\eta \sim e^2 \int_T^{T_{3/2}} d\omega \text{Re} \int_{1/T_0}^{\eta_{\max}} d\eta \frac{g}{\eta} \frac{\ln \frac{\Sigma_\infty^Z + i\Sigma_\infty^{\varphi,T}}{\Sigma_\infty^Z + i\Sigma_\infty^{\varphi,T}}}{\eta [\Sigma_\infty^Z - \Sigma_\infty^Z + i\Sigma_\infty^{\varphi,T} - i\Sigma_\infty^{\varphi,T}]}, \quad (4.36)$$

where $\eta_{\max} = g^2 / \max\{\Sigma_\infty^Z, \Sigma_\infty^{\varphi,T}\}$ is related to the infrared momentum cutoff of the bare interaction propagator, which is established by the characteristic diffuson momenta q .

Using Eqs. (4.26) and (4.29), we find for $\eta \gg 1/T_0$,

$$\Sigma_\infty^Z - \Sigma_\infty^Z \sim g/\eta,$$

$$\Sigma_\infty^{\varphi,T} - \Sigma_\infty^{\varphi,T} \sim gT \ln(\eta_{\max}/\eta). \quad (4.37)$$

For relevant values of $1/T_0 \lesssim \eta \lesssim \eta_{\max}$, these differences arising due to the vertex interaction terms in the diffuson self-energies are small compared to $\Sigma_\infty^Z, \Sigma_\infty^{\varphi,T}$ which simplifies the expression for the conductivity correction,

$$\delta\sigma^H \sim e^2 \text{Re} \int_T^{g^{3/2}T_0} d\omega \int_{1/T_0}^{\eta_{\max}} d\eta \frac{g}{\eta} \frac{1}{\Sigma_\infty^Z + i\Sigma_\infty^{\varphi,T}}. \quad (4.38)$$

For higher frequencies, $T^{3/2}/T_0^{1/2} \ll \omega \ll T_{3/2}$, the Z-factor self-energy Σ^Z is larger than $\Sigma^{\varphi,T}$, while for lower frequencies, $T_0 < T \lesssim \omega \lesssim T^{3/2}/T_0^{1/2}$, the dephasing part dominates. The result reads

$$\delta\sigma^H = \mathcal{O}(1)e^2 \left\{ g^{1/2} - \left(\frac{T}{T_0} \right)^{1/2} \left[1 + \frac{1}{2} \ln \frac{T_1}{T} \right] \right\}, \quad (4.39)$$

where the temperature dependence arises because dephasing strongly suppresses the frequencies $\omega \lesssim T^{3/2}/T_0^{1/2}$ in the Hartree correction.

A schematic overview of the result in the different temperature ranges is shown in Fig. 12. In this plot, we also show the results for the exchange contribution¹⁷

$$\delta\sigma^{\text{ex}} = - \frac{e^2}{(2\pi)^2} \begin{cases} \ln^2(T\tau), & T \gg T_0 \\ 4 \ln g \ln(1/T\tau), & T \ll T_0. \end{cases} \quad (4.40)$$

Most remarkably, while the positive Hartree contribution is larger than the negative exchange contribution over a wide range of temperatures, at low temperatures ($T \ll T_0$), the exchange contribution dominates the temperature dependence again.

D. Dephasing at strong coupling: Weak localization and mesoscopic conductance fluctuations

Let us now turn to the dephasing rate of the Cooperon and UCF diffuson. The path-integral calculation of Sec. III A is modified by inclusion of the Z factor in the Cooperon propagators in Eq. (3.19). In the presence of time-reversal symmetry, the relevant Cooperons are given by disconnected diffusons \tilde{D}_∞ which contain the renormalization part of the self-energy Σ_∞^Z , given by Eq. (4.15).

In this section, we will concentrate on the lowest- T limit, $T \ll T_0$; the generalization onto the case of higher temperatures is straightforward. For $\omega \ll T_0$, in the strong-coupling regime, $\lambda^2 g \gg 1$, we have $Z(\omega) \approx (3\lambda^2 g / 2\pi) \ln(T_0/\omega) \gg 1$, which implies that one should replace ω by $Z\omega \gg \omega$ in all the Cooperon denominators in Eq. (3.19) [in the argument of the logarithm in $Z(\omega)$, the frequency can be replaced by its characteristic value, $\omega \sim 1/t$]. This amounts to the rescaling of frequency $\omega \rightarrow Z\omega$ (inducing the prefactor $1/Z$ from the integration measure $d\omega$) and of the time variable $t \rightarrow t/Z$. The return probability is then given by

$$\tilde{C}(t) = \frac{1}{Z} C^{(0)}(t/Z) = \frac{1}{Z} \frac{Z}{4\pi Dt} = \frac{1}{4\pi Dt}, \quad (4.41)$$

so that the corresponding prefactor in the dephasing action [Eq. (3.18)] is not changed by the renormalization.

As a result of the rescaling, we get from Eq. (3.26),

$$\Delta \tilde{S}^{\text{eff}}(t) \approx 3\lambda^2 g T \frac{t}{Z(t)} \ln \left[\frac{T}{T_0} \frac{t}{Z(t)\tau} \right] \approx \frac{3\lambda^2 g T t}{(3/2\pi)\lambda^2 g \ln(T_0 t)} \ln \frac{Tt}{\lambda^2 g T_0 \tau} \approx 2\pi T t \frac{\ln(gTt/\lambda^2)}{\ln(T_0 t)}. \quad (4.42)$$

From the condition $\Delta \tilde{S}^{\text{eff}}(t \sim \tilde{\tau}_\varphi) \sim 1$, we obtain the characteristic dephasing rate in the strong-coupling regime

$$\frac{1}{\tilde{\tau}_\varphi} \sim T \frac{\ln(g/\lambda^2)}{\ln(T_0/T)}. \quad (4.43)$$

We see that the conductance enters the dephasing rate only under the logarithm: in the realistic case of $\lambda=1$, the Cooperon dephasing rate is given by temperature up to logarithmic factors. This conclusion remains valid in the strong-coupling regime also for the time decay of the diffusons involved in the mesoscopic conductance fluctuations and in

the second-loop weak-localization correction. It is also worth noticing that in the limit of $t \rightarrow \infty$, the dephasing action becomes

$$\Delta\tilde{S}^{\text{eff}}(t \rightarrow \infty) \approx 2\pi Tt. \quad (4.44)$$

On the other hand, the characteristic dephasing length (L_φ) is not affected by the frequency renormalization. Indeed, the dephasing length is the static object, which is defined by the Cooperon at $\omega=0$. The term Dq^2 in the Cooperon denominator is not renormalized by interaction, in contrast to $-i\omega$, so that the renormalization effects related to the Z factor are absent at $\omega=0$. To extract the dephasing length L_φ , one has to compare Dq^2 at $q \sim 1/L_\varphi$ with Σ_∞^φ ,

$$L_\varphi \sim \sqrt{D/\Sigma_\infty^\varphi} \sim L_T/g^{1/2} \ll L_T, \quad (4.45)$$

where $L_T=(D/T)^{1/2}$ is the thermal length. The dephasing length L_φ is thus directly determined by the dephasing part of the Cooperon self-energy Σ_∞^φ and not by the dephasing rate $1/\tilde{\tau}_\varphi \sim \Sigma_\infty^\varphi/Z$.

Therefore, while the dephasing rate is moderate ($1/\tau_\varphi \sim T$) in the strong-coupling regime, the dephasing length is anomalously short ($L_\varphi \ll L_T$). Note that the standard interference experiments (e.g., measuring the magnetoconductivity) usually directly probe the dephasing length rather than the dephasing rate.

The situation when $\tau_\varphi \sim 1/T$ but L_φ and L_T are parametrically different is an indicator of strong renormalization that may occur in strongly correlated systems and in the vicinity of quantum critical points (in particular, at the Anderson transition in the presence of electron-electron interactions²⁷).

In the context of gauge-field models, a related physics has been encountered in Refs. 10 and 11, where the case of rapidly fluctuating gauge fields has been considered. This case may be realized in the gauge-field formulation of the t - J model of high-temperature superconductors, with two species of pseudoparticles, holons, and spinons. There the electric charge is carried by holons, while a fictitious gauge-field effecting the projection onto the physical part of the Hilbert space is controlled by the spinons. The spinons are scattered much more weakly by impurities than the holons, thus allowing the anomalous skin effect regime with typical gauge-field frequency $\omega \propto q^3$ to be reached at sufficiently high temperatures. In that regime, the gauge-field fluctuations lead to a spatially nonuniform diffusion coefficient. As a consequence, the phase breaking length varies with temperature as $L_\varphi \propto T^{-1/6}$, while the relevant time scale for phase breaking processes is still given by the inelastic scattering rate, $1/\tau_\varphi \sim T$. This behavior has been seen in experiment.⁵²

V. UNSCREENED COULOMB INTERACTION

Finally, we contrast the results of Secs. II–IV with a calculation for the case of a long-range electron-electron interaction. The aim of this section is to point out how the different (less singular) gauge-field propagator modifies the quantities of interest. We use the susceptibility⁶

$$\chi(k) = \chi_0 + \frac{e^2 v(k)}{(2\pi\tilde{\phi})^2}, \quad (5.1)$$

with the 2D unscreened Coulomb interaction $v(k)=2\pi e^2/k$, the free-fermion susceptibility $\chi_0=e^2/12\pi m$, and the number of attached flux quanta $\tilde{\phi}$, which for the half-filled lowest Landau level is $\tilde{\phi}=2$. While a short-range interaction, $v(k)=\text{const}$, would just renormalize the value of χ , the long-range interaction leads to a less singular behavior of the gauge-field propagator at small k ,

$$U_{\alpha\beta}(\mathbf{k}, \epsilon) = \frac{\delta_{\alpha\beta}^\perp}{\chi(k)k^2 - i\sigma(k)\epsilon} = \frac{\delta_{\alpha\beta}^\perp}{\chi_0\kappa k - i\sigma(k)\epsilon}, \quad k \ll k_F, \quad (5.2)$$

and the corresponding correlator for thermal fluctuations in the static approximation,

$$\langle a_\alpha a_\beta \rangle_{\mathbf{k}, \epsilon} = \frac{T}{\chi(k)k^2} \delta_{\alpha\beta}^\perp 2\pi\delta(\epsilon) \approx \frac{T}{\chi_0\kappa k} \delta_{\alpha\beta}^\perp 2\pi\delta(\epsilon), \quad (5.3)$$

with the inverse screening length

$$\kappa = \frac{e^4}{2\pi\chi_0\tilde{\phi}^2}. \quad (5.4)$$

For the experimentally relevant case of composite fermions, k_F and κ are not independent: $\kappa/k_F=3C_*/2$, with C_* (see Ref. 17) a numerical constant, which is of order 10 according to experiments.⁵³ We will now consider this situation, $\kappa \gtrsim k_F$, to complement the results for the pointlike interaction from the Sec. IV with corresponding results for unscreened interaction.

A. Cooperon dephasing

We will first consider the dephasing within the static approximation. As we discuss below, the latter is justified for not too low temperatures. For the situation that the Coulomb interaction is unscreened for all relevant momenta, $\kappa \gg k_F$, the less singular gauge-field propagator [Eq. (5.3)] should be used instead of Eq. (3.3) in Eq. (3.18). Then, the result is determined by characteristic momenta $k \in [l^{-1}, k_*]$. Here, $k_* \sim \sqrt{mT/C_*}$ is the highest momentum for which the static approximation is valid. Taking into account that the factor D in the interaction vertex of the left diagram of Fig. 6 acquires a k dependence,

$$D(k) \propto \sigma(k) \approx \begin{cases} \sigma_0, & kl \ll 1 \\ 2\sigma_0/kl, & kl \gg 1, \end{cases} \quad (5.5)$$

the equivalent of Eq. (3.19) (the dephasing action within the static approximation) reads

$$\Delta S^{\text{eff}}(t) = 4\pi Dt \frac{4\lambda^2 e^2 DT}{\chi_0} \int \frac{d\omega}{2\pi} \exp\{i\omega t\} \int_0^\infty \frac{qdq}{2\pi} \times \int_{l^{-1}}^{k_*} \frac{kdk}{2\pi} \int_0^{2\pi} \frac{d\phi}{2\pi} \frac{1}{(Dq^2 - i\omega)^2} \frac{1}{\kappa k} \frac{1-2}{kl}, \quad (5.6)$$

which is consistent with the interpolation formula derived in the microscopic calculation of Ref. 18. Compared to Eq. (3.19), we have dropped the second term in brackets, which is important only for the correct low- k cutoff, since in the present case, important k are from the range $k \in [l^{-1}, k_*]$ rather than $k \in [L_\omega^{-1}, l^{-1}]$. The condition $k_* l \gg 1$, which determines the range of validity of the static approximation, holds in the range of relatively high temperatures,

$$T \gg C_*/g\tau. \quad (5.7)$$

Evaluating Eq. (5.6), we find

$$\Delta S^{\text{eff}} = \frac{16\lambda^2}{C_*} T t \ln \frac{gT\tau}{C_*}, \quad T \gg \frac{C_*}{g\tau}, \quad (5.8)$$

which results in the dephasing rate

$$\frac{1}{\tau_\phi} = \frac{16\lambda^2}{C_*} T \ln \frac{gT\tau}{C_*}, \quad T \gg \frac{C_*}{g\tau}. \quad (5.9)$$

Equation (5.9) is a more moderate dephasing rate than the corresponding result [Eq. (3.23)] for the more singular gauge-field propagator [Eq. (3.3) arising from a short-range interaction, since it does not carry the large parameter g in the prefactor.

In the realistic case $\lambda=1$, we find at $T \gg C_*/g\tau$ a dephasing rate $1/\tau_\phi \sim (T/C_*) \ln(gT\tau/C_*)$, which is similar to the result of Sec. IV D. Using the conventional relation $L_\phi = (D\tau_\phi)^{1/2}$ (which is now valid in view of the absence of strong renormalization effects), we get

$$L_\phi \sim (C_*/\ln g)^{1/2} L_T, \quad (5.10)$$

so that the dephasing length L_ϕ is of the order of L_T for realistic parameters. This should be contrasted to the case of short-range interaction (Sec. IV D), where the anomalously short dephasing length, $L_\phi \sim L_T/g^{1/2} \ll L_T$, was obtained.

At lower temperatures, $T \ll C_*/g\tau$, the reduced thermal phase space for inelastic scattering restricts the relevant transferred momenta to the “diffusive range,” $q \ll k \ll l^{-1}$. The static approximation breaks down for such momenta: the fluctuations of the gauge fields become fast on the scale of the dephasing time, yielding for $\lambda=1$,

$$\frac{1}{\tau_\phi} \sim \frac{T^2 g \tau}{C_*^2} \ln \frac{C_*}{gT\tau}, \quad T \ll C_*/g\tau, \quad (5.11)$$

which corresponds to

$$L_\phi \sim L_T^2/l \gg L_T. \quad (5.12)$$

Thus, at $T \ll C_*/g\tau$, we have a standard Fermi-liquid-type situation: $1/\tau_\phi \ll T$ and $L_\phi \gg L_T$. At the lowest temperatures $T \ll C_*^2/g^2\tau$, the dephasing is, in fact, governed by the scalar (density-density) part of the interaction and is the same as in the standard situation,

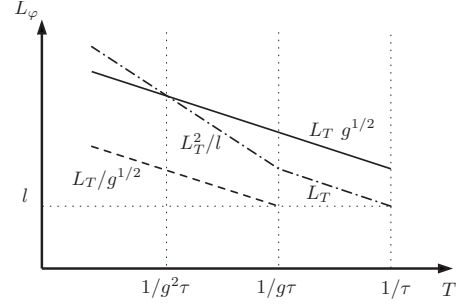


FIG. 13. Schematic plot (log-log scale) of temperature dependence of dephasing length L_ϕ due to gauge-field interaction for the cases of screened (short-range) interaction [dashed line; Eq. (4.45)] and unscreened Coulomb interaction [dashed-dotted line; Eqs. (5.10) and (5.12)]. The conventional dephasing length [Eq. (5.14)] due to the scalar part of interaction (which dominates the lowest- T total dephasing in the unscreened case) is shown by the solid line. For simplicity, the logarithmic factors and C_* are suppressed.

$$\frac{1}{\tau_\phi} \sim \frac{T}{g} \ln g, \quad T \ll C_*^2/g^2\tau, \quad (5.13)$$

with

$$L_\phi \sim L_T g^{1/2} \gg L_T. \quad (5.14)$$

Figure 13 illustrates the behavior of the dephasing length in both the cases of screened (Sec. IV D) and unscreened Coulomb interactions.

B. First-order Hartree correction

We now turn to the evaluation of the effective interaction appearing in the Hartree correction. Since, as we will see below, the behavior of the quantum conductivity corrections is much less dramatic than for the short-range interaction, we set the coupling constant λ to unity in this section. Similar to the dephasing action ΔS^{eff} , the effective interaction box \tilde{U} is now dominated by transferred momenta up to k_F . A calculation accounting for the momentum differences in the Green's functions is given in Appendix F, with the following result to logarithmic accuracy:

$$\tilde{U}(\epsilon=0) = \frac{4}{\pi\nu C_*} \ln g. \quad (5.15)$$

Equation (5.15) results in the following first-order Hartree correction to conductivity:

$$\frac{\delta\sigma^H(T)}{\sigma_0} = \frac{2}{\pi^2 C_* g} \ln g \ln \frac{1}{T\tau}. \quad (5.16)$$

Similar to the dephasing rate [Eq. (5.9)], the correction [Eq. (5.16)] is not as large as in the case of a short-range interaction, since the effective interaction [Eq. (5.15)] is not too strong. For experimentally accessible parameters, the first-order result [Eq. (5.16)] is valid down to exponentially low temperatures.

It should be noted that in addition to the Hartree correction [Eq. (5.16)] and the exchange correction,¹⁷

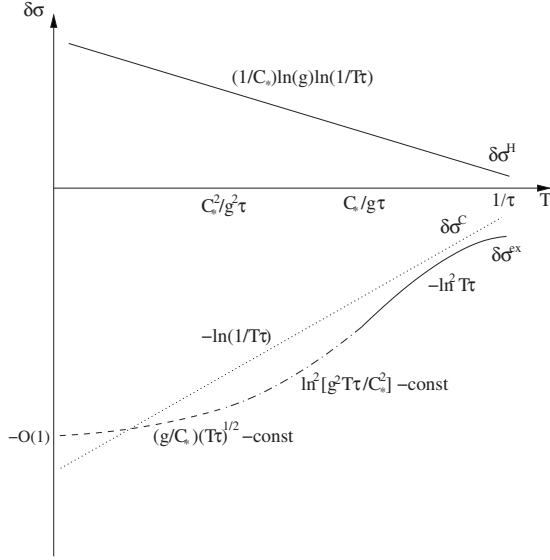


FIG. 14. Schematic plot (log T scale) of the contributions to the conductivity correction for the unscreened Coulomb interaction: the Hartree contribution $\delta\sigma^H$ given by Eq. (5.16), the exchange contribution $\delta\sigma^{ex}$ given by Eq. (19) of Ref. 17, and the standard Altshuler–Aronov contribution $\delta\sigma^C$ due to the scalar Coulomb exchange interaction (Ref. 24). For realistically large conductances $\ln g \ll C_* \ll g$, the exchange term $\delta\sigma^{ex}$ dominates in magnitude over $\delta\sigma^H$ in both magnitude and temperature dependence at $T \gtrsim C_*^2/g^2\tau$, with the dependence in the vicinity of $T \sim C_*/g\tau$ taking the form $\delta\sigma^{ex} \approx -2 \ln(g/C_*) \ln(1/T\tau)$. The temperature dependence of $\delta\sigma^{ex}$ saturates at low temperatures, so that at very low temperatures, the standard contribution $\delta\sigma^C$ becomes dominant. The sum of all contributions is negative for all T , in contrast to the situation of composite fermions with short-range interaction.

$$\delta\sigma^{ex} = -\frac{e^2}{(2\pi)^2} \begin{cases} \ln^2(T\tau), & \frac{C_*}{g\tau} \ll T \ll \frac{1}{\tau} \\ \mathcal{A} - \ln^2\left[\frac{g^2 T\tau}{C_*^2}\right], & \frac{C_*^2}{g^2\tau} \ll T \ll \frac{C_*}{g\tau} \\ \mathcal{A} - \frac{g}{C_*}(T\tau)^{1/2}, & T \ll \frac{C_*}{g^2\tau} \end{cases} \quad (5.17)$$

[with $\mathcal{A} = 2 \ln^2(g/C_*)$], there is also the “standard” Altshuler–Aronov contribution

$$\delta\sigma^C = -\frac{e^2}{2\pi^2} \ln(1/T\tau) \quad (5.18)$$

from the scalar Coulomb interaction.²⁴ Using the experimental parameters of g and C_* for composite fermions in the lowest Landau level, $\delta\sigma^C$ dominates over the Hartree gauge-field contribution over the whole range of temperatures. At very low temperatures, when the gauge-field exchange contribution saturates, it is the “standard” contribution that determines the T dependence of the conductivity (see Fig. 14) for not too large conductance $g < \exp[\pi C_*/4] \sim 1000$, resulting in a negative total correction to the conductivity. In the opposite (purely academic) limit of very high conductances,

the effective coupling constant $\sim \ln(g)/C_*$ becomes larger than unity, leading to an effective Z factor $Z > 1$. In this situation, the resummation scheme of Sec. IV applies.

VI. SUMMARY

We have presented a systematic investigation of the quantum corrections to conductivity in a disordered system of fermions interacting via a fluctuating gauge field, with a focus on the Hartree-type contributions. As a closely related effect, we also analyze the dephasing induced by the gauge-field interaction. We have shown that the anomalously short dephasing length and strong Hartree interaction correction result from the infrared singularity of the gauge-field propagator, arising from a short-range electron-electron interaction.

In general, an important outcome of our analysis is the absence of unphysical divergencies (all the singularities are cut off by disorder). In particular, the results of the paper prove that disorder stabilizes the “mean-field” composite-fermion model of the half-filled lowest Landau level, which in the clean situation suffers from infrared singularities.

For weak coupling $\lambda^2 g \ll 1$ of the fermions to the gauge field discussed in Sec. II, the first-order Hartree conductivity correction [Eq. (2.8)], $\delta\sigma^H \sim \lambda^2 g \ln^2 T$, exceeds the exchange contribution by a large factor g (dimensionless conductance). The correction is found to be finite in the thermodynamic limit at variance with Ref. 22. This is intimately related to the gauge invariance that requires summation of a certain set of the leading-order diagrams (Figs. 2 and 3). In Sec. II B, we elucidate the physical meaning of the obtained contribution and show that it is governed by scattering on static mesoscopic fluctuations of local currents. At exponentially low T , when the first-order correction becomes of the order of the Drude conductivity, we expect that the resummation of higher-order interaction terms would effectively “screen” the $\ln^2 T$ contribution, similarly to the situation of strong coupling discussed in Sec. IV.

In Secs. III A and III B, we discuss dephasing of weak localization and mesoscopic conductance fluctuations at weak coupling. This, in particular, provides the background for the discussion of the dephasing effects on the Hartree correction to conductivity at strong coupling. Within the analysis of dephasing by thermal fluctuations of the gauge field, we have calculated the Cooperon dephasing rate and extended the result of Ref. 18 to a broader temperature range [see Eqs. (3.23), (3.25), and (3.27)]. We have also shown that, similarly to the case of the Coulomb interaction,^{33,39} first-order weak localization and mesoscopic conductance fluctuations are subject to essentially the same dephasing rate [see Eq. (3.32)]. Since this demonstration has been performed on the path-integral level, it also applies to the counterparts of these phenomena in nontrivial geometries, e.g., h/e and $h/2e$ Aharonov–Bohm oscillations. We also have analyzed the dephasing rate applicable to the two-loop weak-localization correction [Eq. (3.47)], which for composite fermions in the half-filled lowest Landau level is the leading one since the first-order Cooperon contribution is absent.

For stronger coupling $\lambda^2 g \gg 1$, an infinite summation of higher-order interaction terms is necessary (see Sec. IV). A

surprisingly rich behavior is found in several distinct temperature regimes, owing to the interplay of the strong dephasing and the renormalization effects. An important ingredient of the theory is the delayed diffuson characterized by large real and imaginary parts of the interaction-induced self-energy [see Eq. (4.24)]. Virtual interaction processes manifest themselves in the delayed-diffuson frequency renormalization by the Z factor in the self-energy: $\Sigma^Z \sim g\omega \gg \omega$. This renormalization effectively leads to the “screening” of the lowest-order contribution to the Hartree correction and dephasing rates.

We have identified two main temperature regimes, which are dominated by (i) strong frequency renormalization by the virtual processes (low temperatures, $T \ll T_0$; Sec. IV B) and by (ii) interplay of renormalization and dephasing (intermediate temperatures, $T_0 \ll T \ll gT_0$; Sec. IV C). The temperature-dependent part of the Hartree conductivity correction is antilocalizing, $d\delta\sigma^H/dT < 0$. At intermediate temperatures, the correction is given by Eq. (4.39) and is parametrically larger than the exchange correction.¹⁷ At lowest temperatures, the temperature-dependent part of the Hartree conductivity correction, Eqs. (4.32) and (4.33), is logarithmically divergent with a prefactor of order unity, $\delta\sigma^H \sim \ln(T_0/T)$. As a result, the negative exchange contribution¹⁷ $\delta\sigma^{\text{ex}} \propto -\ln g \ln(1/T)$ becomes dominant, which yields localization in the limit of $T \rightarrow 0$.

Taking into account the influence of the renormalization processes on dephasing at strong coupling, we show in Sec. IV D that for $\lambda=1$, the dephasing rates are of the order of T : the renormalization of the frequency by virtual processes compensates the large factor of g in the dephasing part of the self-energy. On the other hand, the dephasing length is anomalously short compared to the thermal length, $L_\varphi \sim L_T/g^{1/2} \ll L_T$.

Finally, in Sec. V, we have considered composite fermions that, in addition to the gauge field, interact via the unscreened Coulomb interaction that leads to a less singular gauge-field propagator. As a result, the large parameter g does not appear in the perturbative expressions for the dephasing rate as well as the first-order Hartree correction and the resummation of higher-order gauge-field interaction terms is not needed. At not too low temperatures, the dephasing rate is of the order of the temperature and $L_\varphi \sim L_T$, while at $T \ll gT_0$, we find $L_\varphi \sim L_T^2/l \gg L_T$. For lowest temperatures $T \ll T_0$, the conventional dephasing due to scalar interaction becomes dominant. The Hartree correction [Eq. (5.16)] takes the conventional form, $\delta\sigma^H \propto \ln(1/T)$ (the prefactor is proportional to $\ln g$ but becomes large for unrealistically high conductances only).

On the experimental side, our results have an important implication for composite-fermion systems at half-filling of the lowest Landau level. In view of the parametrically different results for interaction corrections in systems with the Coulomb and short-range interactions at intermediate temperatures, we expect a strong influence of an external gate (located sufficiently close to the 2D gas) on transport properties of the system. Also the dephasing lengths due to gauge-field fluctuations arising from screened or unscreened electron-electron interaction parametrically differ. This should be important for the interpretation of experiments

where interference of composite fermions might be observed. In Ref. 21, a logarithmic temperature dependence of the conductivity has been reported in high-mobility samples. In those samples, most likely the Coulomb interaction was unscreened, so that the Hartree correction was small compared to the exchange contribution. Thus, the interpretation of the experimental data in terms of the gauge-field exchange correction¹⁷ retains its validity.

We close on a more general note. Low-temperature transport and quantum coherence phenomena in strongly correlated systems have become a field of great research interest. The present work, where the interplay of disorder, strong renormalization, and dephasing effects was studied in a system with singular gauge-field interaction, demonstrates the complexity of physics emerging in this context. We expect that the ideas and methods developed here may be useful for the analysis of mesoscopic phenomena in a broad class of strongly correlated systems.

ACKNOWLEDGMENTS

We wish to thank A. R. Akhmerov, V. J. Goldman, J. K. Jain, A. Kamenev, D. V. Khveshchenko, D. L. Maslov, A. Ossipov, P. M. Ostrovsky, D. G. Polyakov, and R. A. Smith for useful discussions. Additionally, we thank D. G. Polyakov for providing the unpublished extended version of Ref. 47. T.L. was supported by the Dutch Science Foundation NWO/FOM. The work of I.V.G., which is conducted as a part of the project “Quantum Transport in Nanostructures” made under the EUROHORCS/ESF EURYI Awards scheme, was supported by funds from the Participating Organizations of EURYI and the EC Sixth Framework Programme. Part of this work was done when three of the authors (T.L., I.V.G., and A.D.M.) participated in the Workshop “Interactions, excitations and broken symmetries in quantum Hall systems” at the Max-Planck-Institut für Physik Komplexer Systeme in Dresden, Germany. T.L. is grateful for the hospitality of the Institut für Nanotechnologie of the Forschungszentrum Karlsruhe and of the Institut für Theorie der Kondensierten Materie of the University of Karlsruhe during several visits while this work was done.

APPENDIX A: EFFECTIVE INTERACTION

In this appendix, we calculate the effective interaction box \tilde{U} given by Eq. (2.5),

$$\tilde{U} = \tilde{U}^{(0)} + \tilde{U}^{(1)} + \tilde{U}^{(2)}, \quad (\text{A1})$$

with the three contributions arising from the three diagrams shown in Fig. 2. Since \tilde{U} is part of the first-order Hartree diagrams, there is no energy transfer through the gauge-field line. The bare box, shown in the left of Fig. 2, is calculated as follows:

$$\begin{aligned}
\tilde{U}^{(0)} &= \frac{1}{(2\pi\nu\tau)^2} \int^{l-1} (dk) U_{\alpha\beta}(\mathbf{k}, \epsilon=0) (e^*)^2 \int (dp) v_{\alpha} v_{\beta} G^R(\mathbf{p}) G^R(\mathbf{p}-\mathbf{k}) G^A(\mathbf{p}) G^A(\mathbf{p}-\mathbf{k}) \\
&= \frac{1}{(2\pi\nu\tau)^2} \int^{l-1} (dk) \frac{(e^*)^2}{\chi_0 k^2} \int (dp) v_x^2 \sin^2 \phi \tau^2 [G^R(\mathbf{p}) G^A(\mathbf{p}-\mathbf{k}) + G^A(\mathbf{p}) G^R(\mathbf{p}-\mathbf{k})] \\
&= \frac{1}{(2\pi\nu\tau)^2} \int^{l-1} (dk) \frac{(e^*)^2}{\chi_0 k^2} 2\tau^2 2\pi i \nu v_F^2 \int \frac{d\phi}{2\pi} \frac{\sin^2 \phi}{(p_F k/m) \cos \phi + i/\tau} \\
&= \frac{1}{(2\pi\nu\tau)^2} \frac{(e^*)^2 v_F^2}{\chi_0} 4\pi\nu\tau^3 \int (dk) \frac{1}{k^2} \frac{1}{1 + \sqrt{1+k^2 l^2}} = 8\pi (e^*)^2 \frac{3g}{\pi\nu} \int (dk) \frac{1}{k^2} \frac{1}{1 + \sqrt{1+k^2 l^2}}, \tag{A2}
\end{aligned}$$

where ϕ is the angle between \mathbf{k} and \mathbf{p} . This integral is determined by small momenta k ,

$$\tilde{U}^{(0)} \approx 2(e^*)^2 \frac{3g}{\pi\nu} \int^{l-1} \frac{dk}{k}. \tag{A3}$$

The boxes with the diffusons crossing the gauge-field line are calculated by expanding both fermionic boxes to the leading order in $ql \ll 1$ and $kl \ll 1$. We find

$$\begin{aligned}
\tilde{U}^{(1)} &= \frac{1}{(2\pi\nu\tau)^2} \int^{l-1} (dk) \\
&\times U_{\alpha\beta}(\mathbf{k}) \frac{1}{(\mathbf{q}-\mathbf{k})^2 - i\omega/D} \frac{(e^*)^2 v_F^2}{2} 2\pi\nu\tau^3 \\
&\times [-4q_{\alpha}q_{\beta} + 2q_{\alpha}k_{\beta} + 2k_{\alpha}q_{\beta} - k_{\alpha}k_{\beta}], \tag{A4}
\end{aligned}$$

$$\begin{aligned}
\tilde{U}^{(2)} &= \frac{1}{(2\pi\nu\tau)^2} \int^{l-1} (dk) \\
&\times U_{\alpha\beta}(\mathbf{k}) \frac{1}{(\mathbf{q}+\mathbf{k})^2 - i\omega/D} \frac{(e^*)^2 v_F^2}{2} 2\pi\nu\tau^3 \\
&\times [-4q_{\alpha}q_{\beta} - 2q_{\alpha}k_{\beta} - 2k_{\alpha}q_{\beta} - k_{\alpha}k_{\beta}]. \tag{A5}
\end{aligned}$$

Here, $\tilde{U}^{(1)}$ and $\tilde{U}^{(2)}$ do not contribute at $k \gg q$, while at $k \ll q$, they cancel the low- k divergence of the bare box $\tilde{U}^{(0)}$: Inserting the sum of the three contributions into the standard exchange diagrams of type $d+e$, the average of the entire diagram (consisting of the effective interaction \tilde{U} times fermionic part \mathcal{B}) over the relative angle ϕ between \mathbf{q} and \mathbf{k} has the structure

$$\begin{aligned}
\langle \tilde{U} \mathcal{B}_{d+e} \rangle_{\phi} &\sim \left\langle \left[\delta_{\alpha\beta} - \frac{k_{\alpha}k_{\beta}}{k^2} \right] \left[\delta_{\alpha\beta} - 4 \frac{q_{\alpha}q_{\beta}}{q^2} \right] q_x q_x \right\rangle_{\phi} \\
&\sim 1 - \langle \cos^2 \phi \rangle - 4 \langle \cos^2 \phi \rangle + 4 \langle \cos^4 \phi \rangle = 0. \tag{A6}
\end{aligned}$$

For the logarithmic accuracy of the calculations of this paper, the details of the low- k cutoff are not important. Since \tilde{U} is always integrated against a fermionic part containing

diffusion propagators, which set $\omega \sim Dq^2$, this also holds for the ω dependence. We may thus apply the low- k cutoff q to the integral in Eq. (A3) and find the effective interaction [Eq. (2.5)].

APPENDIX B: GAUGE INVARIANCE AND EXTRA DIAGRAMS

While calculating the Hartree conductivity correction for the gauge-field problem, one encounters certain cancellations between diagrams, similarly to the case of conventional scalar interaction.²⁴ Such cancellations greatly facilitate the evaluation of $\delta\sigma^H$, as discussed in this appendix.

There are two types of such cancellations. First, all diagrams arising from the variation of the generating functionals shown in Fig. 15 can be combined to zero. This follows from gauge-invariance arguments in the limit of zero gauge-field momentum (the variation of a gauge-invariant functional with respect to a static uniform gauge field must vanish) and has been explicitly demonstrated in Ref. 54. The result is that only diagrams where retarded Green's functions are changed into advanced ones at the external current vertices [“retarded-advanced” (RA) diagrams of type (a) and (b)] remain. This kind of cancellation is used in the strong-coupling regime (Sec. IV), where diagrams of the RA type [(a)+(b)] with interaction-dressed diffusons were evaluated.

An alternative cancellation allows one to take into account only diagrams of types (d) and (e) using the argument of Ref. 24 that the sum of diagrams (a)–(c) is zero in the diffusion approximation. In view of this, the result [Eq. (2.8)] has been calculated from diagrams (d) and (e) (see Fig. 3) in terms of the effective interaction \tilde{U} (Fig. 2).

Let us note that one should exercise certain caution employing this type of cancellation to the gauge-field problem. The point is that additional diagrams with diffusons crossing the gauge-field line, which do not contain the closed effective interaction box \tilde{U} , exist. We show below, however, that these “nonstandard” diagrams cancel out to the leading order. This justifies using the standard diagrams of types (d) and (e) with the effective interaction \tilde{U} for calculating the Hartree correction.

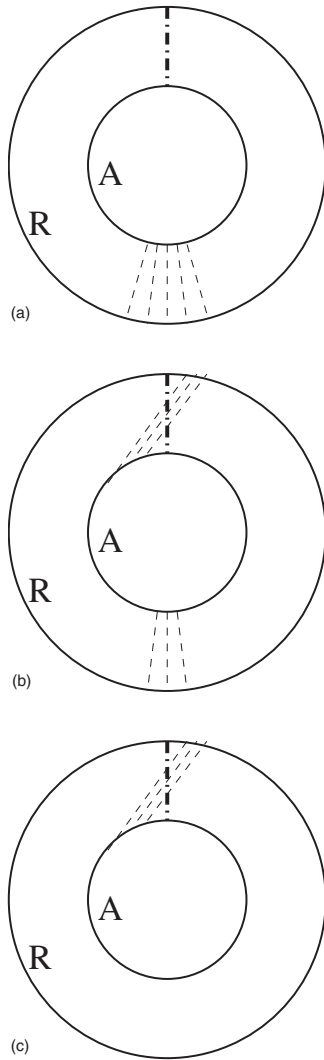


FIG. 15. Generating functionals that lead to the Hartree diagrams. The mirrored versions of diagrams (b) and (c) are also possible.

The extra diagrams can be obtained, along with diagrams of types (c)–(e) and the part of type (a) which contains two retarded (two advanced) Green's functions at the current vertices (RR part) from the generating functionals shown in Fig. 15. The functional without a diffuson crossing the gauge-field line gives the exchange diagrams in terms of the bare part of the effective interaction \tilde{U} , plus diagrams with the velocity vertices next to the interaction vertices, where the latter are small due to an insufficient number of diffusons. However, the functional with the additional diffuson gives, apart from exchange diagrams in terms of the dressed part of \tilde{U} , also relevant diagrams that cannot be classified in terms of \tilde{U} because they do not contain the closed interaction box. In addition, the functional with only the diffuson, which crosses the interaction line, leads to contributions of the same order too.

We start with the diagrams obtained by inserting two velocity vertices into different bubbles of the second functional of Fig. 15. There are 25 possibilities to place the two velocity vertices. In addition, when both vertices are inserted into the

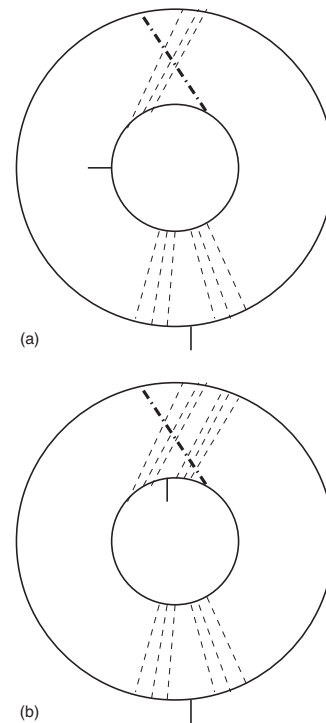


FIG. 16. Examples of diagrams which do not contain the effective interaction \tilde{U} . The diagram (a) has an external current vertex adjacent to the diffuson crossing gauge-field line; the diagram (b) has a velocity vertex splitting the diffuson which crosses the gauge-field line.

same diffuson, the different subpossibilities of placing them have to be taken into account. When placing both vertices in the same bubble, there are 15 possibilities of placing them, which again have to be further distinguished if both vertices are placed in the same diffuson. Of all these possibilities, some contributions are small, some represent the standard diagrams²⁴ in terms of the closed box \tilde{U} , and some give a contribution which is of the leading order but cannot be expressed in terms of \tilde{U} (see two examples in Fig. 16). Also, vertices can be placed splitting the diffuson of the third functional of Fig. 15 (otherwise the contribution is small).

All the remaining contributions that cannot be written in terms of \tilde{U} are only relevant in the case $k \ll q$, since in the opposite case, one or more diffusion poles are displaced by k . Explicitly evaluating the relevant contributions that do not contain \tilde{U} , we find that they cancel and thus do not affect the cancellation of Eq. (A6).

From the second functional of Fig. 15, inserting both velocity vertices into different bubbles so that they split the lower diffuson gives (the part with the dressed gauge-field line of) the standard diagrams of type (c) (if the vertices are not separated by an impurity line) and type (e) (if the vertices are separated by a part of the diffuson), in terms of \tilde{U} . Similarly, inserting the vertices into the lower diffuson into the same bubble gives part of the standard diagrams of type (d) and the RR part of type (a). Evaluated in the limit $k \ll q$, it can be explicitly seen that these diagrams cancel.

APPENDIX C: PATH-INTEGRAL TRANSFORMATION BETWEEN WEAK LOCALIZATION AND MESOSCOPIC CONDUCTANCE FLUCTUATIONS

In this appendix, we present the details of the path-integral transformation that results in Eq. (3.32). For convenience, only the diffuson part of the conductance fluctuations will be considered, assuming that the time-reversal symmetry is broken by random or uniform magnetic field or that

harmonics of the Aharonov–Bohm effect are considered, the amplitude of which is solely determined by the diffuson part.¹⁹

We consider here the weak-coupling situation, $\lambda^2 g \ll 1$, resulting in $l, L_T \ll L_\varphi$: In this case, the regime of interest is $T \gg D/L^2$, and function (3.30) can be approximated by a delta function. For a static gauge-field configuration $\mathbf{a}(\mathbf{r})$, the amplitude of mesoscopic conductance fluctuations can be written as

$$\begin{aligned} \langle \delta g^2 \rangle &= \frac{16\pi D^2}{3TL^4} \int \mathbf{d}^d \mathbf{R}_1 \int \mathbf{d}^d \mathbf{R}_2 \int_0^\infty dt \int_{\mathbf{r}_1(0)=\mathbf{R}_2}^{\mathbf{r}_1(t)=\mathbf{R}_1} \mathcal{D}[\mathbf{r}_1(t)] \int_{\mathbf{r}_2(0)=\mathbf{R}_2}^{\mathbf{r}_2(t)=\mathbf{R}_1} \mathcal{D}[\mathbf{r}_2(t)] \\ &\times \left\langle \exp \left\{ - \int_0^t dt'_1 \left[\frac{\dot{\mathbf{r}}_1^2(t'_1)}{4D} + i\lambda e \dot{\mathbf{r}}_1(t'_1) [\mathbf{a}_1[\mathbf{r}_1(t'_1)] - \mathbf{a}_2[\mathbf{r}_1(t'_1)]] \right] - \int_0^t dt'_2 \left[\frac{\dot{\mathbf{r}}_2^2(t'_2)}{4D} + i\lambda e \dot{\mathbf{r}}_2(t'_2) [\mathbf{a}_1[\mathbf{r}_2(t'_2)] - \mathbf{a}_2[\mathbf{r}_2(t'_2)]] \right] \right\} \right\rangle. \end{aligned} \quad (\text{C1})$$

Clearly, a static gauge field, $\mathbf{a}_1 = \mathbf{a}_2$, drops out of Eq. (C1). In the opposite limit of the time between measurements being long compared to the gauge-field dynamics, correlators between different measurements vanish, i.e., $\langle \mathbf{a}_1 \mathbf{a}_2 \rangle = 0$. Performing the average over Gaussian variables $\mathbf{a}(\mathbf{r})$ results in 16 gauge-field-induced terms in the exponent. Half of them correlates gauge fields from the same measurement, so that in the static approximation discussed in the main text, the result is

$$\begin{aligned} \langle \delta g^2 \rangle &= \frac{16\pi D^2}{3TL^4} \int \mathbf{d}^d \mathbf{R}_1 \int \mathbf{d}^d \mathbf{R}_2 \int_0^\infty dt \int_{\mathbf{r}_1(0)=\mathbf{R}_2}^{\mathbf{r}_1(t)=\mathbf{R}_1} \mathcal{D}[\mathbf{r}_1(t)] \int_{\mathbf{r}_2(0)=\mathbf{R}_2}^{\mathbf{r}_2(t)=\mathbf{R}_1} \mathcal{D}[\mathbf{r}_2(t)] \\ &\times \exp \left\{ - \int_0^t dt' \left[\frac{\dot{\mathbf{r}}_1^2(t')}{4D} + \frac{\dot{\mathbf{r}}_2^2(t')}{4D} \right] - \lambda^2 e^2 \int_0^t dt'_1 dt'_2 \left[\dot{\mathbf{r}}_1(t'_1) [\langle \mathbf{a}[\mathbf{r}_1(t'_1)] \mathbf{a}[\mathbf{r}_1(t'_2)] \rangle + \langle \mathbf{a}_2[\mathbf{r}_1(t'_1)] \mathbf{a}_2[\mathbf{r}_1(t'_2)] \rangle] \dot{\mathbf{r}}_1(t'_2) \right. \right. \\ &+ \dot{\mathbf{r}}_2(t'_1) [\langle \mathbf{a}[\mathbf{r}_2(t'_1)] \mathbf{a}[\mathbf{r}_2(t'_2)] \rangle + \langle \mathbf{a}_2[\mathbf{r}_2(t'_1)] \mathbf{a}_2[\mathbf{r}_2(t'_2)] \rangle] \dot{\mathbf{r}}_2(t'_2) - \dot{\mathbf{r}}_1(t'_1) [\langle \mathbf{a}[\mathbf{r}_1(t'_1)] \mathbf{a}[\mathbf{r}_2(t'_2)] \rangle + \langle \mathbf{a}_2[\mathbf{r}_1(t'_1)] \mathbf{a}_2[\mathbf{r}_2(t'_2)] \rangle] \dot{\mathbf{r}}_2(t'_2) \\ &\left. \left. - \dot{\mathbf{r}}_2(t'_1) [\langle \mathbf{a}[\mathbf{r}_2(t'_1)] \mathbf{a}[\mathbf{r}_1(t'_2)] \rangle + \langle \mathbf{a}_2[\mathbf{r}_2(t'_1)] \mathbf{a}_2[\mathbf{r}_1(t'_2)] \rangle] \dot{\mathbf{r}}_1(t'_2) \right\}. \end{aligned} \quad (\text{C2})$$

Using the transformation

$$\mathbf{r}(t') = \begin{cases} \mathbf{r}_1(t+t'), & -t \leq t' \leq 0 \\ \mathbf{r}_2(t-t'), & 0 \leq t' \leq t, \end{cases} \quad (\text{C3})$$

this is equal to the path-integral representation of the weak-localization correction in a static random gauge field $\mathbf{a}(\mathbf{r})$ after rescaling the gauge-field correlator by a factor 2,

$$\begin{aligned} \langle \delta g^2 \rangle &= \frac{16\pi D^2}{3TL^4} \int \mathbf{d}^d \mathbf{R} \int_0^\infty dt \int_{\mathbf{r}(-t)=\mathbf{R}}^{\mathbf{r}(t)=\mathbf{R}} \mathcal{D}[\mathbf{r}(t)] \exp \left\{ - \int_{-t}^t dt' \frac{\dot{\mathbf{r}}^2}{4D} - \lambda^2 e^2 \int_{-t}^t dt'_1 dt'_2 \dot{\mathbf{r}}(t'_1) [\langle \mathbf{a}[\mathbf{r}(t'_1)] \mathbf{a}[\mathbf{r}(t'_2)] \rangle] \dot{\mathbf{r}}(t'_2) \right\} \\ &= \frac{16\pi D^2}{3TL^4} \int \mathbf{d}^d \mathbf{R} \int_0^\infty dt \int_{\mathbf{r}(-t)=\mathbf{R}}^{\mathbf{r}(t)=\mathbf{R}} \mathcal{D}[\mathbf{r}(t)] \exp \left\{ - \int_{-t}^t dt' \frac{\dot{\mathbf{r}}^2}{4D} \right\} \left\langle \exp \left\{ - 2i\lambda e \int_{-t}^t dt' \dot{\mathbf{r}}(t') \frac{1}{\sqrt{2}} \mathbf{a}[\mathbf{r}(t')] \right\} \right\rangle. \end{aligned} \quad (\text{C4})$$

For thermal gauge-field fluctuations, this is equivalent to rescaling the temperature by a factor of 2 resulting in Eq. (3.32). The different short-scale cutoffs³³ have been discussed in the main text.

APPENDIX D: DIFFUSON SELF-ENERGY

In this appendix, we calculate the delay-time dependent diffuson self-energy Σ_η^Z used in Secs. IV B and IV C. Since in Sec. IV B, the Hartree structure of the contribution to the conductivity correction is ensured by subtracting the disconnected part, here we take into account all possible virtual

contributions to the effective interaction box (the diagrams in Fig. 10 plus the vertex part given by the first diagram in Fig. 2). Similarly to the situation in Appendix A, where the diffusons crossing the gauge-field line set the low-momentum cutoff, the low-momentum cutoff for the self-energy contributions of Fig. 10 is set by corresponding diagrams with a

diffuson covered by the impurity line. In the following, we will therefore only consider the bare boxes with the appropriate cutoff $k \geq q$.

We start with the evaluation of the self-energy of the disconnected diffuson \tilde{D}_∞ at low frequencies $\omega \ll T_0$. Because these frequencies are smaller than the characteristic width of the gauge-field propagator T_0 , the interaction vertices may change retarded into advanced Green's functions. As a result, the three contributions shown in Fig. 10 (and the correspond-

ing ones with the gauge-field line inserted into the advanced Green's function) are possible. The second and third diagrams of Fig. 10 form a Hikami box (see, e.g., Refs. 29 and 50 for discussion of Hikami-box contributions to the self-energy), which combines to one-half the second diagram, while the fourth diagram simply acts as a low- k cutoff for the first one, similarly to the second and third diagrams in Fig. 2 for the first diagram there. We find the following result for the self-energy of the disconnected diffuson,

$$\begin{aligned} \Sigma_\infty^Z = & -2\pi i\nu \frac{1}{(2\pi\nu\tau)^2} \int (dp) \int (dk) \lambda^2 e^2 v_\alpha v_\beta \left[\int_{-\infty}^E \frac{d\epsilon}{2\pi} (G^R)^3 G^A + \frac{1}{2} \int_E^\infty \frac{d\epsilon}{2\pi} (G^R)^2 (G^A)^2 + \int_{E-\omega}^\infty \frac{d\epsilon}{2\pi} G^R (G^A)^3 \right. \\ & \left. + \frac{1}{2} \int_{-\infty}^{E-\omega} \frac{d\epsilon}{2\pi} (G^R)^2 (G^A)^2 \right] (-i) \text{Re } U_{\alpha\beta}(\mathbf{k}, \epsilon). \end{aligned} \quad (\text{D1})$$

Similarly to the calculation of the vertex interaction part in Appendix A, we get (neglecting $E \ll \omega$)

$$\begin{aligned} \Sigma_\infty^Z = & -2\pi i\nu \frac{i}{(2\pi\nu\tau)^2} 2\pi\nu\tau^3 \frac{\lambda^2 e^2 v_F^2}{2} \int_{-\omega}^0 \frac{d\epsilon}{2\pi} \int (dk) \text{Re} \frac{1}{\chi_0 k^2 - i\sigma_0 \epsilon} = -2\pi i\nu \frac{i}{(2\pi\nu\tau)^2} 2\pi\nu\tau^3 \frac{\lambda^2 e^2 v_F^2}{2} \frac{\omega}{2\pi} \frac{1}{2\pi\chi_0} \frac{1}{2} \left[\ln \frac{T_0}{\omega} + 1 \right] \\ = & \frac{3}{2\pi} \lambda^2 g \omega \left[\ln \frac{T_0}{\omega} + 1 \right], \quad \omega \ll T_0. \end{aligned} \quad (\text{D2})$$

The renormalization self-energy Σ_∞^Z can be cast in the form

$$\Sigma_\infty^Z = 2\pi\nu \int_0^\omega \frac{d\epsilon}{2\pi} \text{Re } \tilde{U}(\epsilon), \quad (\text{D3})$$

with

$$\text{Re } \tilde{U}(\epsilon) = \frac{2}{(2\pi\nu)^2 T_0} \int_q^{k_F} k dk \frac{k^2 l^2 (1 + \sqrt{1 + k^2 l^2})}{[k^2 l^2 (1 + \sqrt{1 + k^2 l^2})]^2 + (2\epsilon/T_0)^2}. \quad (\text{D4})$$

Evaluating the momentum integral in Eq. (D4) leads to Eq. (4.3).

For the fully dressed diffuson \tilde{D}_η it is straightforward to see that at zero delay time, the vertex contribution (first diagram of Fig. 2, now with the energy transfer through the gauge-field line integrated over the interval $[-\omega, 0]$ set by the RA channel) exactly cancels with the self-energy [Eq. (D2)].

For the fully dressed diffuson at finite delay time, we account for the partial cancellation with the vertex terms by inserting the factor $[1 - \cos \epsilon\eta]$ [see also Sec. III C and Eq. (4.7)] into the ϵ integral in Eqs. (D2) and (D3) and find

$$\Sigma_\eta^Z = \frac{3}{2\pi} \lambda^2 g \int_{-\omega}^0 d\epsilon \ln \frac{T_0}{|\epsilon|} [1 - \cos \epsilon\eta] = \frac{3}{2\pi} \lambda^2 g \omega \left[\ln \frac{T_0}{\omega} \left(1 - \frac{\sin \omega\eta}{\omega\eta} \right) + 1 - \frac{\text{Si}(\omega\eta)}{\omega\eta} \right],$$

with $\text{Si}(x)$ the integral sine function.

We now turn to the situation of high frequencies, $\omega \gg T_0$. Starting from Eq. (D1), we now allow for the situation of larger energy transfers, thus taking into account contributions from $k \gg l^{-1}$. Neglecting ω and \mathbf{q} in the arguments of the Green's functions, we find

$$\begin{aligned}
\Sigma_{\infty}^Z = & -2\pi i\nu \frac{1}{(2\pi\nu\tau)^2} \int (dp) \int (dk) \lambda^2 e^2 v_{\alpha} v_{\beta} \left[\int_{-\infty}^E \frac{d\epsilon}{2\pi} [G^R(E, \mathbf{p})]^2 G^R(E - \epsilon, \mathbf{p} - \mathbf{k}) G^A(E, \mathbf{p}) \right. \\
& + \int_E^{\infty} \frac{d\epsilon}{2\pi} [G^R(E, \mathbf{p})]^2 G^A(E - \epsilon, \mathbf{p} - \mathbf{k}) G^A(E, \mathbf{p}) - i\tau \int_E^{\infty} \frac{d\epsilon}{2\pi} [G^R(E, \mathbf{p})]^2 G^A(E - \epsilon, \mathbf{p} - \mathbf{k}) \\
& + \int_{E-\omega}^{\infty} \frac{d\epsilon}{2\pi} G^R(E, \mathbf{p}) [G^A(E, \mathbf{p})]^2 G^A(E - \epsilon, \mathbf{p} - \mathbf{k}) + \int_{-\infty}^{E-\omega} \frac{d\epsilon}{2\pi} G^R(E, \mathbf{p}) G^R(E - \epsilon, \mathbf{p} - \mathbf{k}) [G^A(E, \mathbf{p})]^2 \\
& \left. + i\tau \int_{-\infty}^{E-\omega} \frac{d\epsilon}{2\pi} G^R(E - \epsilon, \mathbf{p} - \mathbf{k}) [G^A(E, \mathbf{p})]^2 \right] (-i) \text{Re } U_{\alpha\beta}(\mathbf{k}, \epsilon). \tag{D5}
\end{aligned}$$

Using the relation $G^R G^A = i\tau [G^R - G^A]$ and neglecting the energy differences in the arguments of the Green's functions, this can be simplified to the form analogous to Eq. (D2),

$$\begin{aligned}
\Sigma_{\infty}^Z = & -2\pi i\nu \frac{1}{(2\pi\nu\tau)^2} \int (dk) \frac{\lambda^2 e^2 v_F^2}{2} [-2\pi\nu\tau^3] \\
& \times \frac{2}{1 + \sqrt{1 + k^2 l^2}} \int_{-\omega}^0 \frac{d\epsilon}{2\pi} (-i) \frac{1}{\sigma(k)} \\
& \times \frac{k^2 l^2 T_0 (1 + \sqrt{1 + k^2 l^2}) / 2}{[k^2 l^2 T_0 (1 + \sqrt{1 + k^2 l^2}) / 2]^2 + \epsilon^2}. \tag{D6}
\end{aligned}$$

The factor $2/[1 + \sqrt{1 + k^2 l^2}]$ arises from the momentum difference in the combination $G^R(p)G^A(p-k)$ and is derived in detail in Appendix F. It is canceled by the k dependence of $\sigma(k)$. At $\omega \gg T_0$, Eq. (D6) therefore is dominated by the high-momentum part. It can be calculated as follows:

$$\begin{aligned}
\Sigma_{\infty}^Z = & \frac{2\lambda^2}{\nu} \int_{-\omega}^0 \frac{d\epsilon}{2\pi} \int (dk) \frac{\frac{1}{2}k^2 l^2 T_0 (1 + \sqrt{1 + k^2 l^2})}{[\frac{1}{2}k^2 l^2 T_0 (1 + \sqrt{1 + k^2 l^2})]^2 + \epsilon^2} \\
= & \frac{\lambda^2}{8\pi g \tau} \int_{-\omega/T_0}^0 dy \int_0^{\infty} dz \frac{\frac{z}{2}(1 + \sqrt{1+z})}{[\frac{z}{2}(1 + \sqrt{1+z})]^2 + y^2} \\
= & \frac{\lambda^2}{8\pi g \tau T_0} \int_0^{\infty} d\bar{z} \arctan \left\{ \frac{2}{\bar{z}(1 + \sqrt{1 + \bar{z}\omega/T_0})} \right\} \\
= & \begin{cases} \frac{3}{2\pi} \lambda^2 g \omega \pi \left(\frac{4T_0}{\omega} \right)^{1/3}, & \omega \gg T_0 \\ \frac{3}{2\pi} \lambda^2 g \omega \left[\ln \frac{T_0}{\omega} + 1 \right], & \omega \ll T_0, \end{cases} \tag{D7}
\end{aligned}$$

both confirming Eq. (D2) and providing the behavior for larger ω . Again, it is straightforward to see that at zero delay time, the vertex contribution exactly cancels Eq. (D6).

To calculate the self-energy of the fully dressed diffuson at high frequencies and finite-delay time, we again insert the factor $[1 - \cos \epsilon\eta]$ into Eq. (D6). We first calculate the result for short delay times, $\eta \ll 1/\omega$,

$$\begin{aligned}
\Sigma_{\eta}^Z = & \frac{\lambda^2}{\nu} \int_{-\omega}^0 \frac{d\epsilon}{2\pi} \frac{1}{2} (\epsilon\eta)^2 \int (dk) \frac{\frac{1}{2}k^2 l^2 T_0 (1 + \sqrt{1 + k^2 l^2})}{[\frac{1}{2}k^2 l^2 T_0 (1 + \sqrt{1 + k^2 l^2})]^2 + \epsilon^2} \\
= & \frac{\lambda^2}{8\pi g \tau} \frac{1}{2} (T_0 \eta)^2 \int_{-\omega/T_0}^0 dy y^2 \int_0^{\infty} dz \frac{\frac{z}{2}(1 + \sqrt{1+z})}{[\frac{z}{2}(1 + \sqrt{1+z})]^2 + y^2} \\
\approx & \frac{\lambda^2}{8\pi g \tau} (T_0 \eta)^2 \int_{-\omega/T_0}^0 dy y^2 \int_{2^{2/3}|y|^{2/3}}^{\infty} dz z^{-3/2} \\
= & \frac{\lambda^2}{8\pi g \tau} (T_0 \eta)^2 \frac{3}{8} \left(\frac{2\omega}{T_0} \right)^{8/3} = \mathcal{O}(1) \lambda^2 g \omega (\omega \eta)^2 \left(\frac{T_0}{\omega} \right)^{1/3},
\end{aligned}$$

$$\eta \ll 1/\omega. \tag{D8}$$

For long delay times, $\eta \gg 1/\omega$, the long- η tail of the self-energy can be obtained by extending the limits of the integration over the cosine contribution from $[E - \omega, E]$ to $[-\infty, \infty]$ and evaluating it using the residue theorem,

$$\begin{aligned}
\Sigma_{\eta}^Z = & \Sigma_{\infty}^Z - \frac{\lambda^2}{8\pi g \tau} \int_0^{\infty} dz \pi \exp \left\{ -\frac{1}{2} T_0 \eta z (1 + \sqrt{1+z}) \right\} \\
= & \begin{cases} \Sigma_{\infty}^Z - 3\lambda^2 g T_0 2^{-1/3} \Gamma(5/3) (T_0 \eta)^{-2/3}, & T_0 \eta \ll 1 \\ \Sigma_{\infty}^Z - 3\lambda^2 g / \eta, & T_0 \eta \gg 1. \end{cases} \tag{D9}
\end{aligned}$$

The results of this appendix are summarized in Eqs. (4.15), (4.25), and (4.26). A similar calculation gives also the dephasing part Σ_{η}^{φ} of the self-energy [Eqs. (4.27) and (4.29)]. The only difference is in using $\text{Im } \tilde{U}(\epsilon)$ instead of $\text{Re } \tilde{U}(\epsilon)$ and in a thermal factor [Eq. (4.18)] that is used instead of $\tanh[(\epsilon + \omega)/2T] - \tanh[\epsilon/2T]$.

APPENDIX E: LOW-TEMPERATURE HARTREE CORRECTION

In this appendix, we calculate the Hartree conductivity correction at low temperatures, $T \ll T_0$. We start with the contribution of low frequencies, $T \lesssim \omega \ll T_0$ [note that the function $fz(T_0/\omega)$ exactly drops out],

$$\begin{aligned}
\delta\sigma^{\omega < T_0} &= \sigma_0 \int_{-T_0}^{T_0} \frac{d\omega}{2\pi} \frac{\partial}{\partial\omega} \left[\omega \coth \frac{\omega}{2T} \right] \int_{-\infty}^{\infty} d\eta \int (dq) \frac{1}{2\pi\nu} [\tilde{\mathcal{D}}_\eta - \tilde{\mathcal{D}}_\infty] = \frac{e^2}{4\pi^3} \int_0^{T_0} d\omega \frac{\partial}{\partial\omega} \left[\omega \coth \frac{\omega}{2T} \right] \int_0^{\infty} d\eta \ln \frac{\omega + \Sigma_\infty^Z}{\omega + \Sigma_\eta^Z} \\
&\approx \frac{e^2}{4\pi^3} \int_0^{T_0} d\omega \frac{\partial}{\partial\omega} \left[\omega \coth \frac{\omega}{2T} \right] \int_0^{\infty} d\eta \ln \frac{\Sigma_\infty^Z}{\Sigma_\infty^Z \left[1 - \frac{\sin \omega \eta}{\omega \eta} \right] + \delta\Sigma_\eta^Z}, \tag{E1}
\end{aligned}$$

with

$$\delta\Sigma_\eta^Z = \frac{3\lambda^2}{2\pi} g \omega \left[\frac{\sin \omega \eta}{\omega \eta} - \frac{\text{Si}(\omega \eta)}{\omega \eta} \right]. \tag{E2}$$

Since $\delta\Sigma_\eta^Z$ is only important for $\eta \gtrsim 1/\omega$, this can be written as

$$\begin{aligned}
\delta\sigma^{\omega < T_0} &\approx \frac{e^2}{4\pi^3} \int_0^{T_0} d\omega \frac{\partial}{\partial\omega} \left[\omega \coth \frac{\omega}{2T} \right] \left[\frac{1}{\omega} \int_0^{\infty} dx \ln \frac{1}{1 - \frac{\sin x}{x}} + \int_{1/\omega}^{\eta_{\max}} d\eta \frac{\frac{3}{2\pi} g \omega \text{Si}(\omega \eta)}{\omega \eta \Sigma_\infty^Z} \right] \\
&\approx \frac{e^2}{4\pi^3} \int_0^{T_0} d\omega \frac{\partial}{\partial\omega} \left[\omega \coth \frac{\omega}{2T} \right] \left[\frac{1}{\omega} c_1 + \int_{1/\omega}^{\eta_{\max}} \frac{d\eta}{\eta} \frac{\pi/2}{\omega \left(1 + \ln \frac{T_0}{\omega} \right)} \right] \\
&= \frac{e^2}{4\pi^3} \int_0^{T_0} d\omega \frac{\partial}{\partial\omega} \left[\omega \coth \frac{\omega}{2T} \right] \left[\frac{1}{\omega} c_1 + \frac{\pi \ln g}{2\omega \left(1 + \ln \frac{T_0}{\omega} \right)} \right] = \frac{e^2}{4\pi^3} \left[c_1 \ln \frac{T_0}{T} + \frac{\pi}{2} \ln g \ln \left(\ln \frac{T_0}{T} + 1 \right) \right], \tag{E3}
\end{aligned}$$

which results in Eq. (4.32). Here, η_{\max} is given by the low- k cutoff which is set by the dressed boxes containing extra diffusons, which occurs on the scale $Dq^2 \sim \Sigma_\infty^Z$, so that $\eta_{\max} \sim 1/[q^2 l^2 T_0] \sim 1/[\Sigma_\infty^Z \tau T_0] \sim 1/[g \omega \tau T_0 \ln(T_0/\omega)]$. The numerical constant c_1 is given by the integral

$$c_1 = \int_0^{\infty} dx \ln \frac{1}{1 - \frac{\sin x}{x}}. \tag{E4}$$

APPENDIX F: EFFECTIVE INTERACTION BOX FOR UNSCREENED COULOMB INTERACTION

In this appendix, we calculate the effective interaction \tilde{U} , given by the diagrams in Fig. 2, for the less singular gauge-field propagator [Eq. (5.2)] corresponding to the unscreened Coulomb interaction between the fermions. As mentioned in the main text, relevant transferred momenta are now $k \in [l^{-1}, k_F]$, so that we only need the bare interaction box. Neglecting the diffusive momentum q and the energy transfer ϵ through the gauge-field line, the effective interaction is

$$\begin{aligned}
\tilde{U} &= \frac{1}{(2\pi\nu\tau)^2} (dk) \frac{e^2}{\chi_0 \kappa k} \int (dp) v_x^2 \sin^2 \phi G^R(\mathbf{p}) G^R(\mathbf{p} - \mathbf{k}) G^A(\mathbf{p}) G^A(\mathbf{p} - \mathbf{k}) \\
&= \frac{1}{(2\pi\nu\tau)^2} \int (dk) \frac{e^2}{\chi_0 \kappa k} \int (dp) v_x^2 \sin^2 \phi \tau^2 [G^R(\mathbf{p}) G^A(\mathbf{p} - \mathbf{k}) + G^A(\mathbf{p}) G^R(\mathbf{p} - \mathbf{k})] \\
&= \frac{1}{(2\pi\nu\tau)^2} \int (dk) \frac{e^2 v_F^2}{\chi_0 \kappa k} 2\tau^2 2\pi i \nu \int \frac{d\phi}{2\pi} \frac{\sin^2 \phi}{(p_F k/m) \cos \phi + i/\tau} = \frac{1}{(2\pi\nu\tau)^2} \int (dk) \frac{e^2 v_F^2}{\chi_0 \kappa k} \frac{4\pi\nu\tau^3}{1 + \sqrt{1 + k^2 l^2}}. \tag{F1}
\end{aligned}$$

Performing the momentum integration, we get, within the logarithmic accuracy,

$$\tilde{U} \approx \frac{1}{(2\pi\nu\tau)^2} 4\pi\nu\tau^3 \frac{e^2 v_F^2}{2\pi\chi_0\kappa l} \int_{l^{-1}}^{k_F} \frac{dk}{k} = \frac{12g}{\pi\nu\kappa l} \ln g, \quad (\text{F2})$$

which is Eq. (5.15) of the main text. The last factor in Eq. (F1), which interpolates between small and large k , is the precise version (for particular disorder scattering model) of the interpolation factor in Eq. (21) of Ref. 18, where it was derived for the dephasing action.

-
- *Also at A.F. Ioffe Physico-Technical Institute, 194021 St. Petersburg, Russia.
- †Also at Petersburg Nuclear Physics Institute, 188300 St. Petersburg, Russia.
- ¹T. Holstein, R. E. Norton, and P. Pincus, Phys. Rev. B **8**, 2649 (1973); M. Yu. Reizer, *ibid.* **40**, 11571 (1989); G. Baym, H. Monien, C. J. Pethick, and D. G. Ravenhall, Phys. Rev. Lett. **64**, 1867 (1990).
- ²D. V. Khveshchenko and P. C. E. Stamp, Phys. Rev. Lett. **71**, 2118 (1993); D. V. Khveshchenko and P. C. E. Stamp, Phys. Rev. B **49**, 5227 (1994); B. L. Altshuler, L. B. Ioffe, and A. J. Millis, *ibid.* **50**, 14048 (1994); Y. B. Kim, A. Furusaki, X.-G. Wen, and P. A. Lee, *ibid.* **50**, 17917 (1994); A. Stern and B. I. Halperin, *ibid.* **52**, 5890 (1995).
- ³G. Baskaran and P. W. Anderson, Phys. Rev. B **37**, 580 (1988); L. B. Ioffe and A. I. Larkin, *ibid.* **39**, 8988 (1989); N. Nagaosa and P. A. Lee, Phys. Rev. Lett. **64**, 2450 (1990); P. A. Lee and N. Nagaosa, Phys. Rev. B **46**, 5621 (1992).
- ⁴A. Lopez and E. Fradkin, Phys. Rev. B **44**, 5246 (1991).
- ⁵J. K. Jain, Phys. Rev. Lett. **63**, 199 (1989).
- ⁶B. I. Halperin, P. A. Lee, and N. Read, Phys. Rev. B **47**, 7312 (1993).
- ⁷A. Lopez and E. Fradkin, in *Composite Fermions*, edited by O. Heinonen (World Scientific, Singapore, 1998).
- ⁸S. Simon, in *Composite Fermions*, edited by O. Heinonen (World Scientific, Singapore, 1998).
- ⁹A. G. Aronov, A. D. Mirlin, and P. Wölfle, Phys. Rev. B **49**, 16609 (1994).
- ¹⁰A. G. Aronov and P. Wölfle, Phys. Rev. Lett. **72**, 2239 (1994).
- ¹¹A. G. Aronov and P. Wölfle, Phys. Rev. B **50**, 16574 (1994).
- ¹²A. G. Aronov, E. Altshuler, A. D. Mirlin, and P. Wölfle, Europhys. Lett. **29**, 239 (1995).
- ¹³A. G. Aronov, E. Altshuler, A. D. Mirlin, and P. Wölfle, Phys. Rev. B **52**, 4708 (1995).
- ¹⁴B. N. Narozhny, I. L. Aleiner, and A. Stern, Phys. Rev. Lett. **86**, 3610 (2001).
- ¹⁵A. D. Mirlin, E. Altshuler, and P. Wölfle, Ann. Phys. (Leipzig) **5**, 281 (1996).
- ¹⁶P. A. Lee, E. R. Mucciolo, and H. Smith, Phys. Rev. B **54**, 8782 (1996).
- ¹⁷A. D. Mirlin and P. Wölfle, Phys. Rev. B **55**, 5141 (1997).
- ¹⁸P. Wölfle, Found. Phys. **30**, 2125 (2000).
- ¹⁹T. Ludwig, Ph.D. thesis, Universität Karlsruhe, 2006.
- ²⁰D. V. Khveshchenko, Phys. Rev. Lett. **77**, 362 (1996).
- ²¹L. P. Rokhinson, B. Su, and V. J. Goldman, Phys. Rev. B **52**, R11588 (1995).
- ²²V. M. Galitski, Phys. Rev. B **72**, 214201 (2005).
- ²³I. V. Gornyi, A. D. Mirlin, and P. Wölfle, Phys. Rev. B **64**, 115403 (2001).
- ²⁴B. L. Altshuler and A. G. Aronov, in *Electron-Electron Interaction in Disordered Conductors*, edited by A. L. Efros and M. Pollak (Elsevier, Amsterdam, 1985), pp. 1–153.
- ²⁵G. Zala, B. N. Narozhny, and I. L. Aleiner, Phys. Rev. B **64**, 214204 (2001).
- ²⁶I. V. Gornyi and A. D. Mirlin, Phys. Rev. B **69**, 045313 (2004).
- ²⁷A. M. Finkel'stein, Zh. Eksp. Teor. Fiz. **84**, 168 (1983) [Sov. Phys. JETP **57**, 97 (1983)]; A. M. Finkel'stein, Z. Phys. B: Condens. Matter **56**, 189 (1984); A. M. Finkel'stein, in *Electron Liquid in Disordered Conductors*, Soviet Scientific Reviews, edited by I. M. Khalatnikov (Harwood, London, 1990), Vol. 14; A. Punnoose and A. M. Finkel'stein, Phys. Rev. Lett. **88**, 016802 (2001).
- ²⁸A. Kamenev and A. Andreev, Phys. Rev. B **60**, 2218 (1999).
- ²⁹Y. Adamov, I. V. Gornyi, and A. D. Mirlin, Phys. Rev. B **73**, 045426 (2006).
- ³⁰I. L. Aleiner, B. L. Altshuler, and M. E. Gershenson, Waves Random Media **9**, 201 (1999).
- ³¹I. V. Gornyi, A. D. Mirlin, and D. G. Polyakov, Phys. Rev. B **75**, 085421 (2007).
- ³²B. L. Altshuler, A. G. Aronov, and D. E. Khmel'nitsky, J. Phys. C **15**, 7367 (1982). Some errors in numerical coefficients are corrected in Ref. 30.
- ³³I. L. Aleiner and Ya. M. Blanter, Phys. Rev. B **65**, 115317 (2002).
- ³⁴A. A. Rukhadze and V. P. Silin, Sov. Phys. Usp. **4**, 459 (1961).
- ³⁵A. Stern, Y. Aharonov, and Y. Imry, Phys. Rev. A **41**, 3436 (1990).
- ³⁶L. P. Gor'kov, A. I. Larkin, and D. E. Khmel'nitskii, Pis'ma Zh. Eksp. Teor. Fiz. **30**, 248 (1979) [JETP Lett. **30**, 228 (1980)].
- ³⁷B. L. Altshuler, D. Khmel'nitskii, A. I. Larkin, and P. A. Lee, Phys. Rev. B **22**, 5142 (1980).
- ³⁸S. Chakravarty and A. Schmid, Phys. Rep. **140**, 193 (1986).
- ³⁹T. Ludwig and A. D. Mirlin, Phys. Rev. B **69**, 193306 (2004).
- ⁴⁰B. L. Altshuler, Pis'ma Zh. Eksp. Teor. Fiz. **41**, 530 (1985) [JETP Lett. **41**, 648 (1985)].
- ⁴¹A. D. Stone, Phys. Rev. Lett. **54**, 2692 (1985).
- ⁴²P. A. Lee and A. D. Stone, Phys. Rev. Lett. **55**, 1622 (1985).
- ⁴³B. L. Altshuler and B. I. Shklovskii, Zh. Eksp. Teor. Fiz. **91**, 220 (1986) [Sov. Phys. JETP **64**, 127 (1986)].
- ⁴⁴P. A. Lee, A. D. Stone, and H. Fukuyama, Phys. Rev. B **35**, 1039 (1987).
- ⁴⁵C. L. Kane, R. A. Serota, and P. A. Lee, Phys. Rev. B **37**, 6701 (1988).
- ⁴⁶C. Texier and G. Montambaux, Phys. Rev. B **72**, 115327 (2005).
- ⁴⁷D. G. Polyakov and K. V. Samokhin, Phys. Rev. Lett. **80**, 1509 (1998).

- ⁴⁸G. Catelani and I. L. Aleiner, *Zh. Eksp. Teor. Fiz.* **127**, 372 (2005) [*JETP* **100**, 331 (2005)].
- ⁴⁹F. Marquardt, J. von Delft, R. A. Smith, and V. Ambegaokar, *Phys. Rev. B* **76**, 195331 (2007); J. von Delft, F. Marquardt, R. A. Smith, and V. Ambegaokar, *ibid.* **76**, 195332 (2007).
- ⁵⁰H.-Y. Kee, I. L. Aleiner, and B. L. Altshuler, *Phys. Rev. B* **58**, 5757 (1998).
- ⁵¹B. N. Narozhny, G. Zala, and I. L. Aleiner, *Phys. Rev. B* **65**, 180202(R) (2002).
- ⁵²T. W. Jing, N. P. Ong, T. V. Ramakrishnan, J. M. Tarascon, and K. Retschnig, *Phys. Rev. Lett.* **67**, 761 (1991).
- ⁵³R. R. Du, H. L. Stormer, D. C. Tsui, L. N. Pfeiffer, and K. W. West, *Solid State Commun.* **90**, 71 (1994); *Phys. Rev. Lett.* **70**, 2944 (1993); V. J. Goldman, B. Su, and J. K. Jain, *ibid.* **72**, 2065 (1994); R. R. Du, H. L. Stormer, D. C. Tsui, A. S. Yeh, L. N. Pfeiffer, and K. W. West, *ibid.* **73**, 3274 (1994); D. R. Leadley, R. J. Nicholas, C. T. Foxon, and J. J. Harris, *ibid.* **72**, 1906 (1994); D. R. Leadley, M. van der Burgt, R. J. Nicholas, C. T. Foxon, and J. J. Harris, *Phys. Rev. B* **53**, 2057 (1996); P. T. Coleridge, Z. W. Wasilewski, P. Zawadzki, A. S. Sachrajda, and H. A. Carmona, *ibid.* **52**, R11603 (1995).
- ⁵⁴B. L. Al'tshuler, A. G. Aronov, A. I. Larkin, and D. E. Khmel'nitskii, *Zh. Eksp. Teor. Fiz.* **81**, 768 (1981) [*Sov. Phys. JETP* **54**, 411 (1981)].